HHS Public Access

Author manuscript

Circ Res. Author manuscript; available in PMC 2025 January 19.

Published in final edited form as:

Circ Res. 2024 January 19; 134(2): 143–161. doi:10.1161/CIRCRESAHA.123.322914.

Mitofusin-2 Regulates Platelet Mitochondria and Function

Shancy Jacob[1], **Yasuhiro Kosaka**[1], **Seema Bhatlekar**[1], **Frederik Denorme**[1], **Haley Benzon**[1], **Alexandra Moody**[1], **Victoria Moody**[1], **Emilia Tugolukova**[1], **Grayson Hull**[1], **Nina Kishimoto**[1], **Bhanu K. Manne**[1], **Li Guo**[2,3], **Rhonda Souvenir**[4], **Brayden J. Seliger**[1], **Alicia S. Eustes**[5], **Kelly Hoerger**[1], **Neal D. Tolley**[1], **Amir N. Fatahian**[6], **Sihem Boudina**[1,6], **David C. Christiani**[7,8], **Yongyue Wei**[9,10], **Can Ju**[11], **Robert A. Campbell**[1,12,13], **Matthew T. Rondina**[1,12,13,14], **E. Dale Abel**[4], **Paul F. Bray**[1,15], **Andrew S. Weyrich**[1,16], **Jesse W. Rowley**[1,12]

[1]Molecular Medicine Program, University of Utah, Salt Lake City, UT

[2]Bloodworks Northwest Research Institute, Seattle, WA

[3]Division of Hematology and Oncology, University of Utah, Seattle, WA

[4]David Geffen School of Medicine and University of California, Los Angeles (UCLA), Health, Los Angeles, CA

[5]University of Iowa, Iowa City, IA

[6]Department of Nutrition and Integrative Physiology, University of Utah, Salt Lake City, UT

[7]Department of Environmental Health, Harvard T.H. Chan School of Public Health, Boston, MA, 02115, USA.

Address for Correspondence: Jesse W. Rowley, Ph.D., Eccles Institute of Human Genetics, University of Utah Health Sciences Center, 15 North 2030 East, Room 4220, Salt Lake City, Utah 84112, jesse.rowley@u2m2.utah.edu.

Author Contributions

S.J designed and performed research, analyzed data, wrote the manuscript
Y.K performed research
S. Bhatlekar designed and performed research, analyzed data
F.D performed research, analyzed data
H.B performed research
A.M performed research
V.M performed research
E.T performed research
G.H performed research
N.K performed research
B. M performed research, analyzed data
L.G performed research
R.S performed research
B.S analyzed data
A.E performed research, analyzed data
K.H performed research
N.T performed research
N. F performed research, analyzed data
S. Boudina designed research
D.C. analyzed data
Y. W. analyzed data
C. J. analyzed data
R.C performed research
M.R designed research
E.D.A designed research
P.B designed research
A.W designed research
J.R. designed and performed research, analyzed data, and wrote the manuscript

Disclosures: The authors declare no conflicts or competing financial interests.

[8]Department of Medicine, Massachusetts General Hospital/Harvard Medical School, Boston, MA, 02115, USA.

[9]Peking University Center for Public Health and Epidemic Preparedness and Response, Beijing, 100191, China.

[10]Key Laboratory of Epidemiology of Major Diseases (Peking University), Ministry of Education, Beijing, 100191, China.

[11]Department of Biostatistics, School of Public Health, Nanjing Medical University, Nanjing, Jiangsu, 211166, China.

[12]Department of Internal Medicine, University of Utah School of Medicine, Salt Lake City, UT

[13]Department of Pathology, University of Utah Heath, Salt Lake City, UT

[14]Department of Internal Medicine and the GRECC, George E. Wahlen VAMC, Salt Lake City, UT

[15]Division of Hematology and Hematologic Malignancies, Department of Internal Medicine, University of Utah, Salt Lake City, UT

[16]Oklahoma Medical Research Foundation (OMRF), Oklahoma City, OK.

Abstract

BACKGROUND: Single nucleotide polymorphisms linked with the rs1474868-T allele (*MFN2* T/T) in the human mitochondrial fusion protein Mitofusin-2 (*MFN2*) gene are associated with reduced platelet *MFN2* RNA expression and platelet counts. This study investigates the impact of MFN2 on megakaryocyte (MK) and platelet biology.

METHODS: Mice with MK/platelet deletion of *Mfn2* (*Mfn2*$^{-/-}$) were generated using Platelet factor 4 (Pf4)-CRE crossed with floxed *Mfn2* mice. Human MKs were generated from cord blood, and platelets isolated from healthy subjects genotyped for rs1474868. *Ex-vivo* approaches assessed mitochondrial morphology, function, and platelet activation responses. *In vivo* measurements included endogenous/transfused platelet lifespan, tail bleed time, transient middle cerebral artery occlusion, and pulmonary vascular permeability/hemorrhage following LPS-induced acute lung injury.

RESULTS: Mitochondria was more fragmented in MKs derived from *Mfn2*$^{-/-}$ mice and from human cord blood with *MFN2* T/T genotype compared to control MKs. Human resting platelets of *MFN2* T/T genotype had reduced MFN2 protein, diminished mitochondrial membrane potential, and an increased rate of phosphatidylserine (PS) exposure during *ex vivo* culture. Platelet counts and platelet lifespan were reduced in *Mfn2*$^{-/-}$ mice accompanied by an increased rate of PS exposure in resting platelets, especially aged platelets, during *ex-vivo* culture. *Mfn2*$^{-/-}$ also decreased platelet mitochondrial membrane potential, basal and activated mitochondrial oxygen consumption rate, reactive oxygen species generation, calcium flux, platelet-neutrophil aggregate formation, and PS exposure following dual agonist activation. Ultimately, *Mfn2*$^{-/-}$ mice showed prolonged tail-bleed times, decreased ischemic stroke infarct size after cerebral ischemia-reperfusion, and exacerbated pulmonary inflammatory hemorrhage following LPS-induced acute lung injury. Analysis of MFN2 SNPs in the Identification of SNPs Predisposing to Altered Acute

Lung Injury Risk study identified a significant association between *MFN2* and 28-day mortality in patients with acute respiratory distress syndrome.

CONCLUSIONS: Mfn2 preserves mitochondrial phenotypes in MKs and platelets and influences platelet lifespan, function, and outcomes of stroke and lung injury.

Graphical Abstract

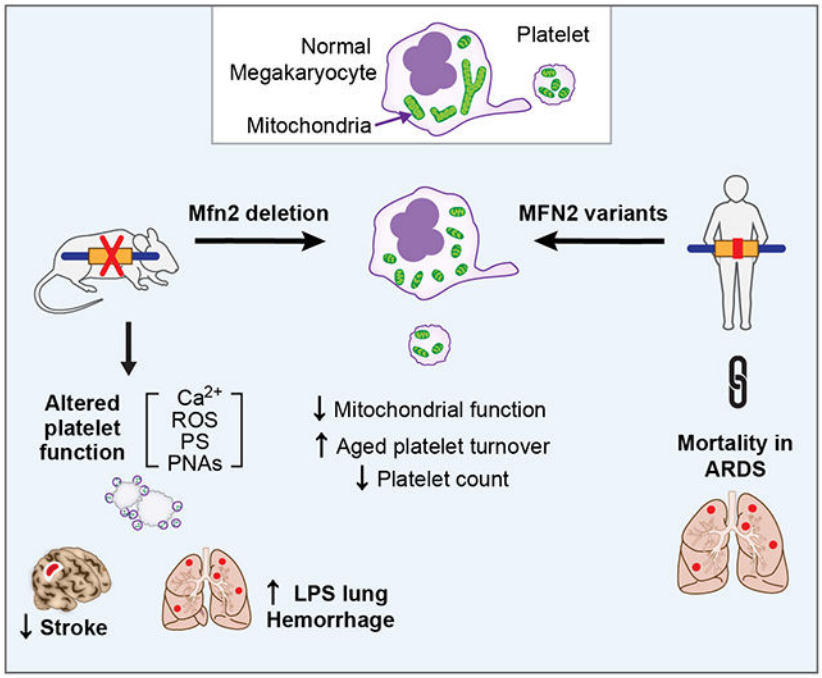

Keywords

Platelet; Megakaryocyte; MFN2; Mitochondria

Subject Terms:

Animal Models of Human Disease; Basic Science Research; Inflammation; Pulmonary Biology; Platelets

Introduction

Heightened reactivity or excessive platelet counts increase the risk of thrombosis, while low platelet counts or reduced reactivity lead to bleeding. Platelet numbers and function also affect normal physiology beyond hemostasis and the pathogenesis of various diseases apart from thrombosis. Underscoring this, a platelet count polygenic risk score was predictive of several diseases and traits of both hematologic and non-hematologic origin including cancer, hypertension, arthritis, inflammation, liver, and kidney function[1]. Even moderate differences in numbers within the normal platelet range are associated with disease[1-3].

Genome wide association studies (GWAS) have associated hundreds of loci with platelet numbers and function[4-7]. Of GWAS loci associated with platelet counts, several are related to mitochondria[6,8], including mitofusin-2 (MFN2). Expression quantitative trait loci (eQTL) in *MFN2* are associated with both platelet counts and *MFN2* mRNA expression in platelets[9,10]. This compelling associative evidence suggests that MFN2 regulates platelet numbers in humans, but a causal role for MFN2 in megakaryocytes (MKs) and platelets has not been established, and the mechanisms and consequences to disease remain unexplored.

Mitochondria exist in dynamic networks of interconnected organelles that are regulated by the balance between mitochondrial fusion and fission[11]. MFN2 and MFN1 are GTPases that promote mitochondrial fusion into inter-connected networks to safeguard mitochondrial integrity and maximize mitochondrial efficiency[11,12]. Platelets rely on uncompromised mitochondria for their survival[13] and normal function[14-16]. They consume large amounts of cellular energy (ATP)[17,18] and mitochondria supply ~30-40% of their basal energy requirements, with the balance supplied by glycolysis[16]. Mitochondrial respiration establishes the mitochondrial membrane potential via the electron transport chain (oxidative phosphorylation (OXPHOS) to generate the proton motive force that drives ATP synthesis. Energy demand, glycolysis, and mitochondrial respiration significantly increase during platelet activation[16,19], and inhibition of mitochondrial respiration reduces platelet activation, degranulation, aggregation, and thrombus formation[16,19,20].

Mitochondria also regulate other modifiers of platelet activation including reactive oxygen species (ROS) and Ca^{2+} homeostasis[21]. These mediate induction of a mitochondrial permeability transition pore (mPTP) essential for the formation of prothrombotic and inflammatory phosphatidylserine+ (PS^{+ve}) procoagulant platelets[22]. Balancing thrombosis with hemostasis, procoagulant platelets prevent microvascular defects and pulmonary bleeding in inflammatory settings[23]. Procoagulant platelets also contribute to coronary artery disease[24] and stroke[25]. Yet, little is known regarding how mitochondrial integrity is preserved during MK development and into circulating platelets.

Among studies that have investigated mitochondrial maintenance in platelets, most have focused on autophagy[26,27] or anti-apoptotic proteins[28]. Here, we use a platelet/MK conditional knockout of Mfn2 in mice (*Mfn2*$^{-/-}$) and human MKs and platelets with the *MFN2* eQTL to investigate the contribution of mitochondrial fusion to platelet numbers and function. We find that Mfn2 promotes platelet survival and function through multiple mitochondrial mechanisms, and that loss of Mfn2 reduces platelet activation, procoagulant platelet (PS^{+ve}) formation, and cerebral injury after ischemic stroke. In an LPS induced acute lung injury (ALI) model, *Mfn2*$^{-/-}$ mice had increased lung vascular permeability that aggravated pulmonary inflammatory bleeding during thrombocytopenia. Analysis of GWAS data from human Acute Respiratory Distress Syndrome (ARDS) patients identified an association between *MFN2* and 28 day mortality.

Materials and Methods

IRB approval:

The study was approved by the University of Utah institutional review board.

Helsinki compliance statement:

The study was conducted in accordance with the Declaration of Helsinki.

Data Availability:

Data will be shared upon reasonable request by the corresponding author: jesse.rowley@u2m2.utah.edu

Human platelet collection

Human blood collection and platelet isolation were performed as previously described[44] using protocols approved by the Institutional Review Board at the University of Utah. See Supplement Table 1 for demographics of human subjects. All donors were healthy. Subjects were excluded if they had used aspirin or any nonsteroidal anti-inflammatory agent within 10 days before the blood draw. Blood was collected by venipuncture into sodium citrate anticoagulant tubes and genotyped for *MFN2* eQTL rs1474868. Whole blood was centrifuged at 180 X g for 20 min to isolate the top layer of platelet-rich plasma. After prostaglandin E1 (PGE1) was added this was centrifuged at 980 X g for 20 min to pellet the platelets. The platelet pellet was washed 3 X with PIPES-saline-glucose buffer (PSG) with PGE1. Washed platelets were used immediately for mitochondrial assessment or pelleted and saved at −80° C for western blot analysis.

MK cultures, *pMFN2* (platelet isoform of MFN2) expression

Mouse MKs were cultured from flushed bone marrow for 4 days in DMEM with TPO as previously described. CD34+ hematopoietic stem cells (HSCs) were isolated from human umbilical vein cord blood. For culturing CD34+ hematopoietic stem cell-derived MKs, human CD34+ cells from human umbilical cord blood were isolated as described previously[71]. The CD34+ cells were cultured in SFEM media supplemented with 40 ng/mL recombinant human stem cell factor (SCF; Invitrogen) and 50 ng/mL recombinant thrombopoietin (TPO; Invitrogen) until day 6 and then 50 ng/mL TPO from days 6-13. The media was replaced every 3 days. RNA was extracted from MKs isolated on days 0, 3, 6, 9, and 13 using Trizol. *pMFN2* was evaluated by semi-quantitative real time PCR using previously published primers[72] (pMfn2-F: CCCAGCTGACCTGTTTATTTG, pMfn2-R: GCGCTCTCCTGGATGTAG, Mfn2-F: GGTGACGTAGTGAGTGTGATG, Mfn2-R: GCAGTGACAAAGTGCTTAAGTG) that we further validated for specificity for real-time PCR by amplification plot and melt curve analysis of *pMFN2* and MNF2 in HeLa and MKs. *MFN2* primers amplified specific products from MKs and HeLa at Ct ~23 whereas *pMFN2* amplified at Ct ~21 and ~32 in MKs and HeLa respectively (not shown). Data was normalized to *GAPDH* and analyzed using the $2^{-\Delta\Delta CT}$ method.

Mitochondria imaging

For imaging, day 13 human MKs or day 4 mouse MKs were plated overnight on fibrinogen coated borosilicate chamber slides. Cells were incubated with 1 μg/mL Hoechts 33342 (ThermoFisher) for 10 min and 100 nM mitotracker green FM (ThermoFisher) for 40 min diluted in growth media without cytokines followed by live imaging on an EVOS FL Auto imaging system equipped with temperature controlled 5% CO_2 incubation

chamber. In our hands, mitochondria were most clear when imaged live with mitotracker dye. To avoid possible mitochondrial changes from prolonged incubation, a rapid visual scoring approach for mitochondrial fusion was implemented. Students who were blinded to experimental conditions were trained to record a single mitochondrial morphology score (1-10) that included a visual approximation of length and branching for each MK as follows. 1: All mitochondria in the MK appeared circular (1X, punctate) with clear separation between mitochondria. 3: mostly circular, some elongated (>3x) mitochondria, little to no branching. 5: some elongated mitochondria (>5x), some branching. 7: mostly elongated (>7x), extensive branching. 10: very elongated (>10x), extensive branching.

Platelet surface PS measurement and platelet imaging

To assess surface PS at baseline (T0), washed platelets were immediately stained with FITC-conjugated annexin V (BioLegend) and CD41-APC (BioLegend) and analyzed by flow cytometry. In parallel experiments, platelets were incubated in M199 at 37° C for 24 h (T24) and stained with FITC-conjugated annexin V and CD41-APC and analyzed by flow cytometry. Washed platelets were fixed with 4% glutaraldehyde and prepared for Transmission Electron Microscopy (TEM) as described previously[73]. Mitochondria were counted and quantified in TEM images by an investigator who was blinded to genotype. For fluorescent microscopy, washed platelets in M199 were added to fibrinogen coated chamber slides and stained live with 100 nM mitotracker deep red for 30 min at 37° C. Media was replaced with 3.7% warm methanol free PFA for 15 min, washed with PBS, permeabilized with ice cold acetone for 5 min, stained with phalloidin 546, and imaged using 60X/1.42 NA oil objective on a confocal-scanning microscope (Olympus IX81, FV300).

Mitochondrial content and potential measurement

Platelet and MK $\Delta\Psi_M$ and mitochondrial content were estimated as described previously[73]. Washed platelets or MKs were incubated with 50 nM tetramethylrhodamine methyl ester (TMRM), mitotracker green FM and anti-CD41 APC in M199 for 20 min at 37° C and analyzed immediately by flow cytometry. Platelets were gated according to FSC/SSC and CD41 expression, and the median fluorescent intensity (MFI) recorded for the gated population. In some experiments, platelets were isolated and analyzed in pairs to decrease variation from technical aspects (especially differences in timing and dye dilution) of the assay.

Mice

All animal experiments complied with the regulatory standards of the University of Utah. Conditional deletion of Mfn2 from platelets in mice (*Mfn2*$^{-/-}$ mice) was achieved by crossing mice harboring a floxed allele of *Mfn2* (*Mfn2*$^{+/+}$)[74] with platelet factor 4-Cre–transgenic mice[75] in which Cre recombinase is expressed under the control of the platelet factor 4 promoter. All experiments were performed using age- and sex-matched 4–6-month-old adult littermates unless otherwise noted.

Immunoblotting

Platelets were lysed in radioimmunoprecipitation assay (RIPA) buffer, protein was mixed with reducing sample buffer and then boiled for 10 min. Proteins were resolved by SDS polyacrylamide gel electrophoresis and transferred to 0.2 μM PVDF (GE Healthcare) or Nitrocellulose membrane (Bio-Rad). Membranes were blocked with 5% non-fat dry milk or LiCor blocking buffer (LiCor Biosciences), incubated with primary and secondary antibodies, and developed using SuperSignal West Pico Plus Chemiluminescent Substrate (Invitrogen) or LiCor Odyssey infrared imaging system. The primary and secondary antibodies used are listed in the major resources table. ImageJ software was used for densitometry quantification.

Platelet counts and turnover

Automated cell counts and MPV measurements were performed on blood collected from the facial vein into microtainer tubes containing K3 EDTA (Sarstedt), using a Hemavet 950 (Drew Scientific). For platelet lifespan, *Mfn2*$^{+/+}$ and *Mfn2*$^{-/-}$ platelets were labelled *in vivo* by intravenous (tail vein) injection of 3.5 μg/mouse of Dylight488-GPIbβ (Emfret Analytics). Blood was collected into ACD by repeated pricking of the lateral tail vein at baseline and at the time points indicated and stained with CD41-APC followed by fixation with BD FACS lysis buffer. The fraction of Dylight488+/CD41+ platelets was assessed by flow cytometer. For regeneration assays, mice were injected with 20 μg of Fc-independent platelet depleting antibody (Emfret R300). Platelet counts were obtained just prior to and at different time points after injection. For platelet mixing and transfusion, *Mfn2*$^{+/+}$ or *Mfn2*$^{-/-}$ donor mice were injected intravenously (tail vein) with 3.5 μg/mouse of Dylight488 or Dylight649-GPIbβ. Blood was harvested 2 h later into ACD by carotid artery cannulation. Blood from a 488 labeled KO mouse was mixed 1:1 with blood from 649 *Mfn2*$^{+/+}$ mouse or vice versa. 100 μL of PBS per mL of blood was added followed by isolation of mixed platelet rich plasma (PRP) by centrifugation. Mixed PRP was injected intravenously (tail vein). Blood was sampled from the facial vein at different time points after injection, stained with CD41-PE and the fraction of 488 versus 649 positive platelets assessed by flow cytometry.

Mouse platelet isolation, activation, and aggregation

Whole blood was drawn into sodium citrate (1:9), diluted to 2 mL with PSG and centrifuged at 150 X g for 8 min. PGE1 was added to the platelet-rich plasma and centrifuged at 400 X g for 8 min. Platelets were counted and resuspended at 4 X 10^8/mL in Tyrode's buffer. For platelet activation, diluted platelets (1 X10^6) were incubated for 10 min at 37° C in the presence of 0, 75 nM and 150 nM PAR4 (Sigma-Aldrich) or 0, 0.025 ng/mL and 1 ng/mL collagen-related peptide (CRP; CambCol Laboratories) with Jon/A-PE (Emfret Analytics), CD62p-FITC (Emfret Analytics) and rat anti-mouse CD41 APC (eBioscience). Reactions were stopped by the addition of FACS lysis buffer (BD biosciences) and analyzed using flow cytometry (BD CytoFLEX). For CM-H_2DCFDA experiments, washed platelets in Tyrode's buffer were loaded with 5 μM 5-(and 6-) chloromethyl-2′, 7′-dichlorodihydrofluorescein diacetate ethyl ester (CM-H_2DCFDA; Invitrogen) at 37° C for 1 h, and then stimulated with 0.1 U/mL thrombin (Sigma-Aldrich) and 500 ng/mL convulxin (CVX; Enzo lifesciences) for

10 min at 37° C. Samples were immediately analyzed by flow cytometry (BD CytoFLEX). For analysis of procoagulant platelet formation washed platelets prepared as described above were resuspended in M199 and stained with rat anti-mouse CD41 APC and FITC-conjugated annexin V and stimulated for 15 min with 0.1 U/mL thrombin and 500 ng/mL CVX (Enzo Lifesciences). Samples were immediately analyzed on BD Cytoflex. For all above assays, platelets were gated according to FSC/SSC and CD41 surface expression to determine the percent positive cells in the gated population. For platelet-neutrophil aggregates, whole blood from *Mfn2*$^{+/+}$ and *Mfn2*$^{-/-}$ mice was drawn in sodium citrate (1:9) and diluted 1:10 in M199 (Lonza) supplemented with 100 U/mL heparin. Diluted whole blood was stained with CD41 APC and rat anti-mouse Ly6G (BioLegend, San Diego, CA) and unstimulated or stimulated with convulxin (6.25 ng/mL or 12.5 ng/mL) for 15 min at 37° C. The samples were fixed with BD FACS lysis buffer and analyzed on a BDCytoflex. Aggregates were defined by FSC/SSC gating and CD41/Ly6G positivity. For all flow cytometry immunostaining, target staining was distinguished from background using isotype antibody controls when necessary. Platelet aggregation was measured with a lumi-aggregometer (Chrono-Log) at 37° C under stirring as previously described. Washed platelets (0.5 mL) were resuspended at 2 X 10^8/mL in Tyrode's buffer (0.5 mL) and were stimulated with collagen (Chrono-Log) or 2MesADP and the change in light transmission was measured.

Platelet mitochondrial function measurements

A 96-well format Seahorse extracellular flux analyzer (Seahorse Bioscience, MA, USA) was used to measure bioenergetics. Washed platelets were diluted to a concentration of 5.5 X 10^7/mL in XF DMEM assay buffer (DMEM with 1 mM pyruvate, 5.5 mM d-glucose, 4 mM l-glutamine, pH 7.4) and 1 X 10^6 platelets were seeded in XF96 microplates and mitochondrial stress test was performed as described previously[15,73]. For some Seahorse experiments, thrombin was injected at 1 U/mL prior to the stress test. ATP content at baseline and after thrombin stimulation was assayed using the ATPlite 1step Luminescence Assay kit (PerkinElmer).

Platelet Ca^{2+} content

Washed platelets at 4 X 10^8 /mL in Tyrode's buffer were labelled with 12.5 μM Fura-2-acetoxymethyl ester (Fura-2AM, Invitrogen) and 0.2% pluronics (Invitrogen) for 45 min at 37° C. The labelled platelets were unstimulated/stimulated with thrombin (0.1 U/mL) and CVX (500 ng/mL) in the presence of 4 mM $CaCl_2$. Fura-2AM fluorescence was measured by excitation at 340 nm and 380 nm and emission was measured at 509 nm using a FlexStation 3 microplate reader (Molecular Devices). The 340/380 ratio of Fura-2 emissions were calculated.

Hemostasis and thrombosis—Tail-bleeding times were measured by clipping 1 mm from the tip of the tail of mice anesthetized with ketamine and xylazine (80/12 mg/kg). The tail was placed in pre-warmed saline at 37^0 C, and the time to cessation of bleeding was measured for 10 min. For $FeCl_3$-induced carotid artery thrombosis model, carotid arteries of anesthetized *Mfn2*$^{+/+}$ and *Mfn2*$^{-/-}$ were exposed to Whatman No. 1 filter paper (1 mm × 1 mm) saturated with freshly prepared 10% FeCl3 (anhydrous) for 2 min. Blood flow

was monitored using a laser Doppler flow probe (moorVMS-LDF1; Moor Instruments) and the time for complete occlusion of blood flow was recorded. Data was censored at 20 minutes. Transient middle cerebral artery occlusion (tMCAO) was performed as described previously[25]. The right middle cerebral artery (MCA) was occluded for 60 min followed by reperfusion for 24 h. Brains slices were stained with 2% 2,3,5-triphenyl tetrazolium chloride (Sigma-Aldrich, St. Louis, MO) and infarct areas (white) were quantified using ImageJ software (National Institutes of Health, Bethesda, MD).

Acute Lung injury model—LPS-induced acute lung injury models were performed as described previously[23]. Briefly, mice were anesthetized and challenged intratracheally with saline or *Escherichia coli*-derived LPS (O111:B4; Sigma). In some experiments, mice received anti-mouse GPIbα (R300, Emfret Analytics) antibody to deplete platelets 16h prior to LPS challenge. Twenty-four hours later, mice were euthanized by cervical dislocation and bronchoalveolar lavage (BAL) fluid was collected by intratracheal flushing with 3 X 1 mL saline. Subsequently, aliquots of BAL fluids were treated with 2.5% triton X-100 and 0.1 N NaOH to assess hemoglobin by fluorescence absorbance at 405 nM. Protein content in the BAL fluids were quantified by BCA protein estimation method.

GWAS and SKAT analysis of ARDS in humans

GWAS data for ARDS were obtained from the (iSPAAR) consortium study[39,40]. iSPAAR samples were from the Molecular Epidemiology of ARDS (MEARDS) study enrolled at the Massachusetts General Hospital and Beth Israel Deaconess Medical Center and from the ARDS Clinical Trials Network (ARDSNet). In the current study, we imputed the samples using Trans-Omics for Precision Medicine (TOPMED), and after quality control, we retained a total of 2,210 samples (983 cases and 1,227 controls) with complete clinical information, along with over 14 million SNPs.

179 SNPs were selected that mapped within a 500kb range upstream and downstream of MFN2 for the GWAS and SKAT[41] analysis. Specifically, SNPs were screened within 1:11480181-12515211, and among them, 8 SNPs are located in the Exon regions.

In GWAS and SKAT analyses, adjustments included the same set of covariates. For both the platelets model and ARDS risk model, covariates of age, sex, race, trauma, sepsis, blood transfusion, Inhalation injury, pneumonia, and the first 5 principal components were adjusted. For the 28-day mortality model, covariates of age, sex, sepsis, pneumonia, apache score, and the first 5 principal components were adjusted. SKAT analysis[41] was used to comprehensively consider interactions between multiple SNPs in MFN2 and platelet count, ARDS risk, and 28 day mortality. Full results of the GWAS and SKAT analysis can be found in the supplemental dataset.

Statistics

Statistics were calculated in GraphPad Prism 9 and R version 4.0.4. Assumption of Normality was assessed with Shapiro-Wilk and Kolmogorov-Smirnov tests. For samples with normality test P values > 0.05, two group testing was performed using paired or unpaired two-tailed student t-test as indicated. ANOVA and unpaired t-tests were used

for multi-group significance testing followed by adjustment where indicated for multiple comparisons. For samples with normality test $P < 0.05$, or with small sample size ($n < 10$), Mann-Whitney and Kruskal Wallis tests were used for two group and multi-group comparisons. For comparisons with small sample sizes and large effect sizes, a nonparametric bootstrap test with pooled resampling was used (1000 bootstrap resamples)[76]. In all tests P-value < 0.05 was considered significant. The two independent cohorts in Figure 7 and Supplement Figure 9 were independently analyzed and individual p-values reported. P-values were combined for meta-analysis using the method of Stouffer (sumz) in the R package metap[77] with weights proportional to the square root of the sample size. Individual data points, the significance test used, and sample sizes are reported in each figure or legend. For each figure, representative images were subjectively selected that best illustrated the differences identified by the quantitative results.

Results

Conditional deletion of Mfn2 in mouse MKs and platelets alters mitochondrial phenotypes

To establish a causal role for MFN2 in modulating platelet counts, and further explore the function of Mfn2 in platelets and MKs, we generated platelet/MK specific *Mfn2* knockout mice (called hereafter $Mfn2^{-/-}$) (Figure 1A). Western blot analysis confirmed Mfn2 protein was present in $Mfn2^{+/+}$ but absent in $Mfn2^{-/-}$ mouse platelets (Figure 1B). Mfn1 protein, which was low in abundance and difficult to detect in mouse platelets, also appeared reduced by $Mfn2^{-/-}$, whereas the inner mitochondrial membrane fusion protein Opa1 and the fission protein Drp1 remained unchanged (Supplement Figure 1). Mitochondrial morphology was visually different in cultured bone marrow megakaryocytes from $Mfn2^{-/-}$ compared to control mice (Figure 1C). Scoring of mitochondrial morphology for fusion (see Figure 6C and methods) by observers blinded to the conditions of the experiment indicated a significant shift toward punctate, fragmented mitochondria in $Mfn2^{-/-}$ MKs compared to control MKs (Figure 1D). Mitotracker staining in platelets (Figure 1E) showed visibly more punctate mitochondria compared to megakaryocytes. The regular presence of comparably elongated mitochondria in cultured megakaryocytes and proplatelet extensions (Supplement Figure 2) compared to platelets indicates active mitochondrial fission just prior to or after platelet release, as suggested by a recent study[29]. Differences in mitochondrial length were not readily apparent between $Mfn2^{+/+}$ and $Mfn2^{-/-}$ platelets (Figure 1E) as they were with megakaryocytes imaged with mitotracker at the same resolution. Quantitation of mitochondria area and perimeter in high resolution single plane TEM slices also did not indicate significant differences between $Mfn2^{+/+}$ and $Mfn2^{-/-}$ platelets (Supplement Figure 3A-B), but we suspect that more subtle differences in mitochondrial size may manifest when imaged in 3 dimensions, at a higher resolution, and with more sophisticated quantitation. Most mitochondria in single plane slices were round or oval as in the example images in Figure 1F, although rare longer mitochondria were captured by TEM in both $Mfn2^{+/+}$ and $Mfn2^{-/-}$ platelets (Supplement Figure 3C). We did not find evidence by TEM of altered platelet morphology, cristae structure, autophagy, or ER-mitochondrial contact sites (data not shown). However, manual counts of mitochondria in single plane TEM images indicated a shift toward fewer mitochondria per $Mfn2^{-/-}$ platelet section (Supplement Figure 3D-E).

Staining with the dye TMRM indicated lower mitochondrial membrane potential ($\Delta\Psi_M$) in Mfn2 deficient mouse platelets compared to control platelets (Figure 2A and Supplement Figure 4A), whereas the staining intensity of mitotracker was unchanged (Figure 2B). Seahorse assays were used to measure oxygen consumption rate (OCR) as a readout of oxidative phosphorylation (mitochondrial respiration) and ATP production **(see** supplement Figure 4B-C). As shown in Figure 2C-D, unstimulated platelets from *Mfn2*$^{-/-}$ mice had lower basal and maximal OCR, and lower ATP-linked respiration than *Mfn2*$^{+/+}$ platelets. Thrombin treatment increased the OCR in *Mfn2*$^{+/+}$ platelets, but OCR in response to thrombin was significantly blunted in *Mfn2*$^{-/-}$ platelets (Figure 2E-F). Similarly, maximal and ATP linked respiration remained significantly reduced after thrombin treatment in *Mfn2*$^{-/-}$ vs *Mfn2*$^{+/+}$ platelets (Figure 2E-F). On the other hand, basal and thrombin induced extracellular acidification rate (ECAR), which is an index of glycolysis, did not differ between *Mfn2*$^{-/-}$ vs *Mfn2*$^{+/+}$ platelets (Supplement Figure 4D).

Electron transport via mitochondrial complex I is considered a rate limiting step of cellular respiration. Complex I protein Ndufb8, which is essential for the assembly and activity of complex I, was reduced in *Mfn2*$^{-/-}$ platelets compared to *Mfn2*$^{+/+}$ platelets (Figure 2G-H) without a decrease in RNA expression (data not shown) suggesting a defect in complex I assembly. Complex I activity also trended lower (Figure 2I). Expression of other index mitochondrial complex proteins in complexes II-V remained unchanged (Supplement Figure 4E-F), although we were unable to assess the activity of these complexes. Despite reduced mitochondrial complex I and ATP production, there was not a detectable loss of ATP stores in Mfn2 $^{-/-}$ vs control resting or activated platelets (Figure 2J).

Mfn2 deficiency reduces platelet counts through accelerated apoptosis of aging platelets

Consistent with the previously reported association of platelet count and *MFN2* RNA expression in humans, platelet counts in *Mfn2*$^{-/-}$ mice were modestly reduced (Figure 3A). These counts remained lower in *Mfn2*$^{-/-}$ mice although platelet counts rise between 2-6 months as animals age (Supplement Figure 5A). Mean platelet volume (MPV) of *Mfn2*$^{-/-}$ mice was also higher in 3–6-month-old mice (Supplement Figure 5B). Thiazole orange staining of immature reticulated platelets in additional groups of mice indicated a larger fraction of newly generated platelets in *Mfn2*$^{-/-}$ mice (Figure 3B). The number of MKs identified by Von Willebrand Factor (VWF) staining of bone marrow sections (Supplement Figure 6A-B), and the number of bone marrow derived MKs making proplatelets in culture (Supplement Figure 6C-D) remained unchanged between *Mfn2*$^{-/-}$ and control mice. In line with this, the rate of platelet regeneration after depletion was unchanged (Supplement Figure 6E).

In vivo platelet labeling experiments indicated a significant reduction in lifespan of *Mfn2*$^{-/-}$ platelets (Figure 3C), with an overall shorter half-life of 53.4±1.4 hours (mean±SEM) relative to littermate controls (61.1±0.90 hours, mean±SEM) (Figure 3D). To determine if this Mfn2 effect on platelet survival is intrinsic to platelets (rather than for example increased consumption because of bleeding in *Mfn2*$^{-/-}$ mice), we differentially labeled *Mfn2*$^{+/+}$ and *Mfn2*$^{-/-}$ platelets, mixed them together at 50:50, transfused them into *Mfn2*$^{+/+}$ mice, and examined their ratio over time as depicted in Figure 3E. When circulating in

the same animal, the survival of platelets from *Mfn2*$^{-/-}$ mice was reduced relative to the *Mfn2*$^{+/+}$ platelets (Figure 3F-G). At 96 h post transfusion, the average ratio of *Mfn2*$^{-/-}$ platelets to *Mfn2*$^{+/+}$ platelets was reduced to 23:77.

Depolarization of mitochondrial potential precedes caspase-3 activation and PS exposure which marks platelets for rapid clearance from the circulation[30-32]. To address intrinsic platelet apoptosis in the absence of *in vivo* clearance, platelets were incubated *ex vivo* for 16 h at 37° C. To additionally control for potential secondary effects on PS exposure such as from bystander platelet activation, we again dual labeled *Mfn2*$^{+/+}$ and *Mfn2*$^{-/-}$ platelets for co-culture in the same well. After 16 hours culture there was significantly higher surface PS (Annexin V binding) in the *Mfn2*$^{-/-}$ platelets compared to co-cultured control platelets (Figure 3G), suggesting a more rapid intrinsic rate of death. Mitochondrial potential decreased over time in both *Mfn2*$^{+/+}$ and *Mfn2*$^{-/-}$ cultured platelets (Figure 3H), while there was a trend that was not statistically significant, toward accelerated activation of caspase-3 in *Mfn2*$^{-/-}$ platelets (Figure 3I-J, Supplement Figure 7A). However, treatment with Abt-263 (inhibits Bcl-xL[33]) or with H_2O_2 (induces cytochrome c release), induced equivalent levels of PS exposure between *Mfn2*$^{-/-}$ and *Mfn2*$^{+/+}$ platelets (Supplement Figure 7B-C) suggesting mechanisms upstream of cytochrome c and Bak and Bax restraint. A pronounced induction of markers of autophagy/mitophagy was observed by 8 hours of culture, but these did not differ between *Mfn2*$^{+/+}$ and *Mfn2*$^{-/-}$ platelets (Supplement Figure 7D). We then performed experiments to determine the contribution of platelet age to Mfn2 regulated apoptosis. We injected *Mfn2*$^{+/+}$ and *Mfn2*$^{-/-}$ mice with Dylight 488-GPIbα to label platelets, and let the labeled platelets age *in vivo* for 72 h. We analyzed PS exposure on the surface immediately (T0) and after *ex vivo* incubation at 37° C for 8 h (T8) and 14 h (T14) by flow cytometry. As shown in Figure 3K, compared to new platelets, old platelets from both *Mfn2*$^{+/+}$ and *Mfn2*$^{-/-}$ mice demonstrated accelerated PS exposure during *ex vivo* culture. While new *Mfn2*$^{+/+}$ and *Mfn2*$^{-/-}$ platelets did not differ in the extent of PS exposure at any time point during *ex vivo* culture, old *Mfn2*$^{-/-}$ platelets showed significantly higher PS exposure compared to old *Mfn2*$^{+/+}$ platelets after 8 and 14 hours of *ex vivo* culture (Figure 3K). Together, this indicates that platelet turnover and counts are affected by Mfn2 loss through accelerated apoptosis marked by PS exposure in aging platelets.

Loss of Mfn2 impairs platelet activation, procoagulant platelet formation and reduces infarct size in a cerebral ischemia-reperfusion model

Given known roles of mitochondria in platelet activation, we tested the hypothesis that Mfn2 loss would reduce platelet activation. Indeed, *Mfn2*$^{-/-}$ platelets exhibited modestly reduced αIIb/β3 activation (Jon/A) in response to high concentrations of the thrombin receptor agonist PAR4 peptide and collagen receptor agonist CRP (Figure 4A). Alpha-granule release, marked by CD62p (P-selectin) surface translocation did not reach a statistically significant difference between *Mfn2*$^{-/-}$ and *Mfn2*$^{+/+}$ platelets after CRP or PAR4 stimulation (Figure 4B). Compared to controls, *Mfn2*$^{-/-}$ platelets did not display statistically significant differences in aggregation in response to collagen (Figure 4C) or 2-Mes-ADP (Supplement Figure 8A). In *ex vivo* whole blood, *Mfn2*$^{-/-}$ platelets formed less aggregates with neutrophils in response to an intermediate dose of the collagen receptor agonist convulxin (Figure 4D) compared to *Mfn2*$^{+/+}$ platelets.

Inhibition of mitochondrial complex I impairs platelet PS^{+ve} procoagulant platelet formation (see Supplement Figure 8B and [34]). Accordingly, dual agonist stimulated procoagulant platelet formation was significantly reduced in complex I deficient (Figure 2H) *Mfn2*$^{-/-}$ platelets (Figure 4E). However, *Mfn2*$^{-/-}$ did not affect calcium ionophore A23187 stimulated procoagulant platelet formation (Supplement Figure 8C). Complex I and III, contribute to ROS generation, an effector of procoagulant platelet formation. Dual agonist stimulation induced significantly lower levels of ROS in *Mfn2*$^{-/-}$ vs *Mfn2*$^{+/+}$ platelets (Figure 4F). In concert with ROS, procoagulant platelet formation requires a strong and sustained Ca^{2+} flux. As shown in Figure 4G, *Mfn2*$^{-/-}$ impaired thrombin/convulxin stimulated Ca^{2+} flux. Together, the data point to multiple convergent mitochondrial defects affecting platelet activation and PS exposure.

P-selectin, procoagulant platelets, and platelet neutrophil aggregates (PNAs) promote hemostasis and contribute to arterial occlusion, ischemic stroke, and reperfusion injury[25]. As shown in Figure 4H, bleeding was modestly prolonged in *Mfn2*$^{-/-}$ mice compared to *Mfn2*$^{+/+}$ mice following tail tip transection. However, there was not a difference in arterial occlusion time in *Mfn2*$^{-/-}$ vs *Mfn2*$^{+/+}$ mice following ferric chloride injury of the carotid artery (Supplement Figure 8D). On the other hand, *Mfn2*$^{-/-}$ mice had visually reduced cerebral infarcts compared to *Mfn2*$^{+/+}$ mice after transient middle cerebral artery occlusion for 1 h, followed by 23 h of reperfusion (Figure 4I). Infarct volumes were 55±5 mm^3 in *Mfn2*$^{-/-}$ mice compared to 85±3 mm^3 in *Mfn2*$^{+/+}$ mice (Figure 4J). However, the difference in infarct size was not sufficient to cause a measurable difference in motor function or neurological outcomes (data not shown).

Loss of Mfn2 increases lung vascular permeability and aggravates inflammatory bleeding in LPS-induced acute lung injury model

During inflammation, PS^{+ve} procoagulant platelet sentinels maintain hemostasis by preventing leukocyte diapedesis-inflicted microbleeding[23]. Therefore, we hypothesized that MFN2 would be particularly important for vasculoprotection in LPS-induced pulmonary inflammation, which is a model of Acute Respiratory Distress Syndrome (ARDS) during human sepsis[35]. To test this, we performed acute lung injury by intratracheal LPS administration in *Mfn2*$^{+/+}$ and *Mfn2*$^{-/-}$ mice and 24 hours later quantified protein in broncho-alveolar fluid (BALF) as a measure of vascular leakage. With LPS administration alone, *Mfn2*$^{-/-}$ but not *Mfn2*$^{+/+}$ significantly increased protein infiltration in BALF (Figure 5A) compared to saline treated mice, but there was no visual evidence of bleeding in lungs in either *Mfn2*$^{+/+}$ or *Mfn2*$^{-/-}$ mice (data not shown). Thrombocytopenia is known to potentiate pulmonary LPS-induced injury and hemorrhage in mice[23], and moderate to severe thrombocytopenia in humans (~$50x10^9$/L i.e. ~20% of the population mean) is a common sequela of sepsis and acute lung injury that is associated with mortality[36-38]. To model moderate to severe thrombocytopenia in mice co-incident with lung injury, we partially depleted platelets to approximately 20% of normal ($MFN2^{+/+}$: 142±84 $x10^3$/μL; $MFN2^{-/-}$: 219±152 $x10^3$/μL; vs 1055±150 $x10^3$/μL in un-depleted WT mice; mean±SD) in both *Mfn2*$^{+/+}$ and *Mfn2*$^{-/-}$ mice using anti-mouse GPIbα, and performed intratracheal LPS-induced lung injury. Platelet depletion caused LPS induced inflammatory bleeding in both *Mfn2*$^{+/+}$ and *Mfn2*$^{-/-}$ lungs (Figure 5B) with increased hemorrhage visual in lungs from

Mfn2$^{-/-}$ mice compared to littermate *Mfn2*$^{+/+}$ controls (Figure 5B-C). Increased bleeding was also visually evident in the appearance of the BALF (Figure 5D). Accordingly, whereas protein leakage in the lungs of *Mfn2*$^{+/+}$ compared to *Mfn2*$^{-/-}$ did not reach a statistically significant difference (Figure 5E), a statistically significant increase in red blood cell (RBC) infiltration (Figure 5F) was measured in the BALF of MFN2$^{-/-}$ compared to their *Mfn2*$^{+/+}$ littermate controls.

Reduced *pMFN2* expression by the *MFN2* eQTL affects mitochondrial phenotypes in human MKs and platelets

The rs1474868 T allele is linked to a cluster of SNPs across the *MFN2* gene in humans. The rs1474868 T/T genotype is associated with a 17% reduction in mean platelet counts, and a 3-5 fold reduction in expression of a platelet specific isoform of *MFN2* mRNA (*pMFN2*)[9] compared to C/C or C/T genotypes. Consistent with this, the T/T allele strikingly reduced *pMFN2* mRNA expression in MKs from cultured human cord blood CD34+ cells compared to C/C or C/T alleles (Figure 6A). Labeling of human MKs with mitotracker green indicated shorter, more fragmented mitochondria in *MFN2* T/T compared to *MFN2* C/C MKs (Figure 6B). As shown in Figure 6C, the extent of mitochondrial fusion varied widely in individual MKs across both genotypes. On average however, MKs with the *MFN2* T/T eQTL had significantly lower fusion scores compared to their C/C counterparts (Figure 6D).

We confirmed previous reports[9] that platelets from individuals with the T/T genotype of rs1474868 had significantly less *pMFN2* RNA compared to C/C or C/T platelets (Figure 7A) and further found that this corresponded to a significant reduction in total MFN2 protein (Figure 7B). Staining with TMRM indicated lower mitochondrial membrane potential (Figure 7C) but no difference in mitotracker staining in the T/T platelets (Supplement Figure 9A). This translated to a modest increase in the small fraction of depolarized (TMRM-) T/T versus C/C or C/T platelets (Figure 7D). As shown in Figure 7E, a higher percentage of T/T platelets than C/C or C/T platelets exposed PS after 24 hours of *ex vivo* culture suggesting an effect of MFN2 on human platelet survival. The same trend of reduced TMRM and increased PS exposure in T/T platelets after *ex vivo* culture for 48 hours was confirmed in an additional cohort (Supplement Figure 9B-C). Active caspase-3 measured in this cohort at 24 and 48 hours of *ex vivo* culture also trended higher in T/T vs C/C or C/T platelets (Supplement Figure 9D-E). Together, the data suggest that MFN2 modulates mitochondrial network morphology in MKs and survival of human platelets.

Given the contribution of MFN2 to pulmonary hemorrhage following LPS induced lung injury in mice, GWAS data from the iSPAAR consortium ARDS study[39,40] was analyzed by SKAT[41] for possible complex associations between *MFN2* SNPs and platelet count, ARDS risk, and prognosis. SKAT results indicated no statistical significance between *MFN2* and platelet count (P=0.8317) or ARDS risk (P=0.8867). However, *MFN2* was found to be significantly associated with 28-day mortality of ARDS patients (P=0.0424) (Supplement Figure 10 and Supplement dataset 1).

Discussion

We uncovered a mitochondrial role for MFN2 in MKs and platelets using mouse knockout models and cells from humans with *MFN2* polymorphisms. Mitochondrial dysfunction underlies numerous diseases including those where dysregulated hemostasis or thrombosis are significant effectors of morbidity and mortality[20,42-54]. Aging alone (organismal and cellular) results in a gradual decline in mitochondrial function[55,56]. MFN2 and Mitofusin-1 (MFN1) redundantly regulate outer mitochondrial membrane fusion[12] to preserve mitochondrial integrity and function. *MFN2* RNA is abundant in human and mouse platelets, whereas *MFN1* RNA is very low in both species (approximately 20 times less than *MFN2*)[57], although there are reports of MFN1 protein presence in platelets (https://www.thegpm.org/). Dynamin-related protein 1 (DRP1), also abundant in platelets[57], balances MFN-mediated fusion through activating mitochondrial fission[58]. Changes in fusion or fission machinery can tip the balance towards hyperfused or fragmented mitochondria[59]. In line with this, mitochondrial morphology was visibly tipped toward fission in mouse MKs with deletion of Mfn2. Increased fission was also visible in unperturbed human MKs harboring a common *MFN2* genetic variant. The population genotype frequency of rs1474868 T is approximately 50% (Gnomad)[60]. This common allele had a dramatic effect on MK transcript expression, decreasing it by more than 90%, which likely explains the fission phenotype. We were surprised at such a prominent effect for a variant with high allele frequency, but may be feasible because the rs1474868 genotype primarily affects the MK/platelet enriched isoform of MFN2[9]. We can only speculate on the reason for the more pronounced effect of rs1474868 on *pMFN2* in MKs than platelets. As some of the linked variants are in the transcribed region of the isoform, perhaps there are different rates of turnover between mRNA from C vs T alleles in platelets vs in vitro cultured MKs.

As with the human association with reduced *MFN2* RNA expression and platelet counts[6,8], *Mfn2* deletion in MKs caused modestly lower platelet counts in mice. Mouse experiments demonstrated that this was primarily from a difference in platelet survival rather than production. In both humans and mice, MNF2 maintained $\Delta\Psi_M$ and prevented premature caspase-3 activation and PS exposure in resting platelets. PS flipping to the outer leaflet of plasma membrane is regulated by two distinct pathways- the programmed cell apoptosis pathway and the necrotic procoagulant pathway. The former Bak/Bax-caspase pathway plays a central role in regulating the lifespan of circulating quiescent platelets—a major determinant of platelet counts[13]. In mixing experiments, we observed a non-linear, preferential loss of *Mfn2*$^{-/-}$ platelets that accelerated over time as platelets aged in the circulation. This non-linear shift in survival supports the “multiple hit” model[30] of platelet turnover which proposes that anti-apoptotic signals in platelets are eventually overwhelmed by pro-apoptotic signals that accumulate as platelets age[61]. In support of this, we found that circulatory aged platelets were more prone to PS exposure during *ex vivo* culture than younger platelets, and *Mfn2*$^{-/-}$ accelerated PS exposure in circulatory aged but not young platelets. The exact nature of the “multiple hits” to aging platelets and their premature demise in Mfn2 deficiency remains to be determined, but one possibility is energetic exhaustion. We saw a significant loss of mitochondrial respiratory capacity with *Mfn2*

deletion. Interestingly, platelet function and mitochondrial respiratory capacity is known to decline in older platelets allowed to age via Bak/Bax deletion[61].

Fusion of mitochondria maximizes respiration by allowing the rapid distribution of metabolites and electrical coupling over larger continuous stretches of membrane, and supporting the mixing and re-portioning of damaged mitochondria for removal by fission[58]. Thus, without Mfn2, mitochondria functionally decline over time, much like we observed for our platelets. Related to this, complex I levels and activity were reduced in *Mfn2*$^{-/-}$ platelets similar to losses observed with Mfn2 deficiency in other cells[62].

As others have reported, thrombin rapidly increased O_2 consumption in our platelets[15]. This was significantly blunted in the absence of Mfn2. Evidence suggests mitochondrial OXPHOS and ATP is required for maximal platelet integrin activation, granule release, and aggregation to some agonists[63,64] which were all reduced by *Mfn2*$^{-/-}$. Thus, reduced respiration, in concert with decreased ROS generation and Ca^{2+} signaling, likely contribute to the reduced platelet responses.

Stimulation with dual agonists induces mPTP formation, a non-selective multiprotein pore which rapidly dissipates $\Delta\Psi_M$, leads to mitochondrial swelling, and causes procoagulant platelet PS exposure[65]. Mitochondrial ROS and a strong, sustained Ca^{2+} flux are determinants of mPTP formation[66] which were both decreased in *Mfn2*$^{-/-}$ platelets. Complexes I and III are major sites of ROS generation during mitochondrial respiration. Blocking complex I with rotenone or decreasing mitochondrial respiration, as occurs in *Mfn2*$^{-/-}$ platelets, reduces ROS production.

Procoagulant platelets promote arterial and venous thrombosis. P-selectin, PS^{+ve} platelets, and PNAs have been shown to mediate and exacerbate brain injury during ischemic stroke *in vivo*[25]. Platelets lacking cyclophilin D (CypD), a critical regulator of mPTP formation were reported to have lower ability to become PS^{+ve}, form less PNAs, and confer protection against cerebral ischemia-reperfusion injury[25]. Like CypD deficient animals, animals with Mfn2 deficient platelets had reduced infarct size and ischemic stroke volume after cerebral ischemia-reperfusion injury.

Beyond their prothrombotic properties, PS^{+ve} platelets are shown to bind clotting factors and prevent inflammatory bleeding. Thus, PS^{+ve} platelets can become prothrombotic or prevent bleeding depending on the setting. Inflammatory bleeding is marked by loss of vascular integrity due to neutrophil transmigration into inflamed endothelium leading to infiltration of RBCs and plasma contents. Platelets were recently shown to migrate to these vascular breaches, become PS^{+ve} via GPVI and plug the endothelial holes left behind by transmigrating neutrophils[23]. *Mfn2*$^{-/-}$ platelets failed to maintain vascular integrity in LPS-induced acute lung injury and resulted in increased vascular permeability. This defect in the local protective effect of PS^{+ve} platelets was more prominent, especially for *Mfn2*$^{-/-}$ mice, when we depleted their platelets to similar levels and performed LPS-induced acute lung injury. When interpreting these findings is important to note that all Cre-lox mouse models have some degree of leakage into other lineages. Recent studies have firmly demonstrated

leakage of PF4-Cre in macrophages, especially during inflammation[67], and the contribution of Mfn2 in macrophages or other lineages to lung bleeding can't be ruled out.

LPS-induced lung injury is a model for Acute Respiratory Distress Syndrome (ARDS) in humans, a major complication of sepsis where LPS is thought to contribute to lung damage. Previous studies have linked genetic variants affecting platelet counts to ARDS risk and survival[38,68]. Analysis of iSPAAR consortium data[39] did not find individual associations between our marker SNP rs1474868 and platelet counts, ARDS risk, or ARDS outcomes. However, aggregate analysis of SNPs across *MFN2* with SKAT[41] indicated a complex, significant association between *MFN2* variants in humans and survival in ARDS. In line with this, platelet mitochondria are compromised in human sepsis, and mitochondrial potential and respiration are also associated with clinical outcomes[69,70].

Although Mfn2$^{-/-}$ mice recapitulated certain human platelet and MK phenotypes of *MFN2* T/T genotype, differences of mouse models should be considered when interpreting the findings. *MFN2* T/T genotype significantly reduced MFN2 protein in human platelets, whereas protein was absent in *Mfn2*$^{-/-}$ mouse platelets. Further studies using knock-in models will be required to define the exact causal variant in humans and assess the specific effects of this variant. The mitochondrial necessity for platelet survival and function over time may also differ between species since human platelets survive 7-10 days versus 4-6 days in mice. Finally, while lung hemorrhage and bleeding are clearly complications in multiple human diseases, whether procoagulant platelets in humans affects bleeding remains to be determined.

In conclusion, our study reveals an essential mitochondrial role for Mfn2 in regulating multiple facets of mitochondrial phenotypes in MKs and platelets that affect platelet clearance, activation, thrombosis, and bleeding. These newly defined aspects of MFN2 biology in platelets and MKs may be relevant to interpreting previously reported associations between genetic variants in *MFN2* that affect platelet count and disease.

Supplementary Material

Refer to Web version on PubMed Central for supplementary material.

Acknowledgements

We thank Diana Lim and Nikita Abraham for preparation of the figures, critical comments, and consultation regarding effective display of the images. We thank Antoinette Blair and Darian Murray for assistance with participant recruitment. This work was supported by GM103806 and HL144957 (JWR), HL142804 (MTR), NHLBI U54 HL1123 and R35HL145237 (ASW) and American Heart Association Career Development Award (LG). This work was supported in part by Merit Review Award Number I01 CX001696 to MTR from the United States (U.S.) Department of Veterans Affairs Clinical Sciences R&D (CSRD) Service. This material is the result of work supported with resources and the use of core facilities at the University of Utah, Salt Lake City, Utah. The contents do not represent the views of the U.S. Department of Veterans Affairs or the United States Government. The ARDS GWAS datasets were obtained as part of the identification of SNPs Predisposing to Altered ALI Risk (iSPAAR) study funded by the NHLBI (RC2 HL101779).

Nonstandard Abbreviations and Acronyms

MFN2	Mitofusin-2

GWAS	Genome wide association studies
eQTL	Expression quantitative trait loci
MPV	Mean platelet volume
ATP	Adenosine triphosphate
OXPHOS	Oxidative Phosphorylation
MK	Megakaryocyte
ROS	Reactive oxidative species
mPTP	Mitochondrial permeability transition pore
PS	Phosphatidylserine
tMCAO	Transient middle cerebral artery occlusion
LPS	Lipopolysaccharide
ALI	Acute lung injury
ARDS	Acute respiratory distress syndrome
Drp1	Dynamin related protein-1
OPA1	Optic atrophy-1
MFN1	Mitofusin-1
$\Delta\Psi_M$	Mitochondrial membrane potential
TMRM	Tetramethylrhodamine methyl ester
OCR	Oxygen consumption rate
TO	Thiazole Orange
CRP	Collagen related peptide
PAR4	Protease-activated receptor 4
PNA	Platelet neutrophil aggregate
BALF	Bronchoalveolar lavage fluid
SKAT	Sequence kernel association trait
iSPAAR	Identification of SNPs predisposing to altered ALI risk

References

1. Mikaelsdottir E, Thorleifsson G, Stefansdottir L, et al. Genetic variants associated with platelet count are predictive of human disease and physiological markers. Communications Biology 2021 4:1. 2021;4(1):1–13.

2. Vinholt PJ, Hvas AM, Frederiksen H, et al. Platelet count is associated with cardiovascular disease, cancer and mortality: A population-based cohort study. Thromb Res. 2016;148:136–142. [PubMed: 27586589]
3. Bonaccio M. Does platelet count count? Thromb Res. 2016;148:143–144. [PubMed: 27837908]
4. Keramati AR, Chen MH, Rodriguez BAT, et al. Genome sequencing unveils a regulatory landscape of platelet reactivity. Nature Communications 2021 12:1. 2021;12(1):1–13.
5. Eicher JD, Lettre G, Johnson AD. The genetics of platelet count and volume in humans. Platelets. 2018;29(2):125–130. [PubMed: 28649937]
6. Gieger C, Radhakrishnan A, Cvejic A, et al. New gene functions in megakaryopoiesis and platelet formation. Nature. 2011;480(7376):201–8. [PubMed: 22139419]
7. Puurunen MK, Hwang SJ, Larson MG, et al. ADP Platelet Hyperreactivity Predicts Cardiovascular Disease in the FHS (Framingham Heart Study). Journal of the American Heart Association: Cardiovascular and Cerebrovascular Disease. 2018;7(5):.
8. Astle WJ, Elding H, Jiang T, et al. The Allelic Landscape of Human Blood Cell Trait Variation and Links to Common Complex Disease. Cell. 2016;167(5):1415–1429.e19. [PubMed: 27863252]
9. Simon LM, Chen ES, Edelstein LC, et al. Integrative Multi-omic Analysis of Human Platelet eQTLs Reveals Alternative Start Site in Mitofusin 2. Am J Hum Genet. 2016;98(5):883–897. [PubMed: 27132591]
10. Rondina MT, Voora D, Simon LM, et al. Longitudinal RNA-seq analysis of the repeatability of gene expression and splicing in human platelets identifies a platelet selp splice QTL. Circ Res. 2020;126(4):501–516. [PubMed: 31852401]
11. Liesa M, Palacín M, Zorzano A. Mitochondrial dynamics in mammalian health and disease. Physiol Rev. 2009;89(3):799–845. [PubMed: 19584314]
12. Archer SL. Mitochondrial Dynamics — Mitochondrial Fission and Fusion in Human Diseases. New England Journal of Medicine. 2013;369(23):2236–2251. [PubMed: 24304053]
13. Mason KD, Carpinelli MR, Fletcher JI, et al. Programmed anuclear cell death delimits platelet life span. Cell. 2007;128(6):1173–86. [PubMed: 17382885]
14. Wang L, Wu Q, Fan Z, et al. Platelet mitochondrial dysfunction and the correlation with human diseases. Biochem Soc Trans. 2017;45(6):1213–1223. [PubMed: 29054925]
15. Ravi S, Chacko B, Sawada H, et al. Metabolic Plasticity in Resting and Thrombin Activated Platelets. PLoS One. 2015;10(4):.
16. Zharikov S, Shiva S. Platelet mitochondrial function: from regulation of thrombosis to biomarker of disease. Biochem Soc Trans. 2013;41(1):118–23. [PubMed: 23356269]
17. Kramer PA, Ravi S, Chacko B, Johnson MS, Darley-Usmar VM. A review of the mitochondrial and glycolytic metabolism in human platelets and leukocytes: Implications for their use as bioenergetic biomarkers. Redox Biol. 2014;2:206–210. [PubMed: 24494194]
18. Salganicoff L, Fukami MH. Energy metabolism of blood platelets. Arch Biochem Biophys. 1972;153(2):726–735. [PubMed: 4662106]
19. Barile CJ, Herrmann PC, Tyvoll DA, et al. Inhibiting platelet-stimulated blood coagulation by inhibition of mitochondrial respiration. Proc Natl Acad Sci U S A. 2012;109(7):2539–43. [PubMed: 22308457]
20. Randriamboavonjy V, Mann WA, Elgheznawy A, et al. Metformin reduces hyper-reactivity of platelets from patients with polycystic ovary syndrome by improving mitochondrial integrity. Thromb Haemost. 2015;114(3):569–78. [PubMed: 25993908]
21. Carrim N, Arthur JF, Hamilton JR, et al. Thrombin-induced reactive oxygen species generation in platelets: A novel role for protease-activated receptor 4 and GPIbα. Redox Biol. 2015;6:640–7. [PubMed: 26569550]
22. Mattheij NJA, Gilio K, van Kruchten R, et al. Dual mechanism of integrin αIIbβ3 closure in procoagulant platelets. J Biol Chem. 2013;
23. Kaiser R, Escaig R, Kranich J, et al. Procoagulant platelet sentinels prevent inflammatory bleeding through GPIIBIIIA and GPVI. Blood. 2022;140(2):121–139. [PubMed: 35472164]

24. Pasalic L, Wing-Lun E, Lau JK, et al. Novel assay demonstrates that coronary artery disease patients have heightened procoagulant platelet response. J Thromb Haemost. 2018;16(6):1198–1210. [PubMed: 29569428]
25. Denorme F, Manne BK, Portier I, et al. Platelet necrosis mediates ischemic stroke outcome in mice. Blood. 2020;135(6):429. [PubMed: 31800959]
26. Lee SH, Du J, Stitham J, et al. Inducing mitophagy in diabetic platelets protects against severe oxidative stress. EMBO Mol Med. 2016;8(7):779–795. [PubMed: 27221050]
27. Zhang W, Ren H, Xu C, et al. Hypoxic mitophagy regulates mitochondrial quality and platelet activation and determines severity of I/R heart injury. Elife. 2016;5:.
28. Lebois M, Josefsson EC. Regulation of platelet lifespan by apoptosis. Platelets. 2016;27(6):497–504. [PubMed: 27100842]
29. Poirault-Chassac S, Nivet-Antoine V, Houvert A, et al. Mitochondrial dynamics and reactive oxygen species initiate thrombopoiesis from mature megakaryocytes. Blood Adv. 2021;5(6):1706–1718. [PubMed: 33720340]
30. McArthur K, Chappaz S, Kile BT. Apoptosis in megakaryocytes and platelets: the life and death of a lineage. Blood. 2018;131(6):605–610. [PubMed: 29259001]
31. Chen M, Yan R, Zhou K, et al. Akt-mediated platelet apoptosis and its therapeutic implications in immune thrombocytopenia. Proc Natl Acad Sci U S A. 2018;115(45):E10682–E10691. [PubMed: 30337485]
32. Alonzo MTG, Lacuesta TLV, Dimaano EM, et al. Platelet Apoptosis and Apoptotic Platelet Clearance by Macrophages in Secondary Dengue Virus Infections. J Infect Dis. 2012;205(8):1321–1329. [PubMed: 22383677]
33. Debrincat MA, Pleines I, Lebois M, et al. BCL-2 is dispensable for thrombopoiesis and platelet survival. Cell Death & Disease 2015 6:4. 2015;6(4):e1721–e1721.
34. Kholmukhamedov A, Janecke R, Choo HJ, Jobe SM. The mitochondrial calcium uniporter regulates procoagulant platelet formation. Journal of Thrombosis and Haemostasis. 2018;16(11):2315–2321. [PubMed: 30179298]
35. D'Alessio FR. Mouse models of acute lung injury and ARDS. Methods in Molecular Biology. 2018;1809:341–350. [PubMed: 29987799]
36. Assinger A, Schrottmaier WC, Salzmann M, Rayes J. Platelets in sepsis: An update on experimental models and clinical data. Front Immunol. 2019;10(JULY):1687. [PubMed: 31379873]
37. Brooks D, Barr LC, Wiscombe S, et al. Human lipopolysaccharide models provide mechanistic and therapeutic insights into systemic and pulmonary inflammation. European Respiratory Journal. 2020;56(1):.
38. Wei Y, Wang Z, Su L, et al. Platelet Count Mediates the Contribution of a Genetic Variant in LRRC 16A to ARDS Risk. Chest. 2015;147(3):607–617. [PubMed: 25254322]
39. Dong X, Zhu Z, Wei Y, et al. Plasma Insulin-like Growth Factor Binding Protein 7 Contributes Causally to ARDS 28-Day Mortality: Evidence From Multistage Mendelian Randomization. Chest. 2021;159(3):.
40. Christiani DC, Wei Y, Huang H, et al. Association of Serum Mannose With Acute Respiratory Distress Syndrome Risk and Survival. JAMA Netw Open. 2021;4(1):e2034569–e2034569. [PubMed: 33502483]
41. Lee S, Emond MJ, Bamshad MJ, et al. Optimal unified approach for rare-variant association testing with application to small-sample case-control whole-exome sequencing studies. Am J Hum Genet. 2012;91(2):224–237. [PubMed: 22863193]
42. Protti A, Fortunato F, Artoni A, et al. Platelet mitochondrial dysfunction in critically ill patients: comparison between sepsis and cardiogenic shock. Crit Care. 2015;19(1):39. [PubMed: 25757508]
43. Edwards JK. Mitochondrial function in autoimmune disorders. Nat Rev Nephrol. 2016;12(3):126–126. [PubMed: 26782146]
44. Boilard E, Nigrovic PA, Larabee K, et al. Platelets Amplify Inflammation in Arthritis via Collagen-Dependent Microparticle Production. Science (1979). 2010;327(5965):580–583.
45. Birsoy K, Possemato R, Lorbeer FK, et al. Metabolic determinants of cancer cell sensitivity to glucose limitation and biguanides. Nature. 2014;508(7494):108–112. [PubMed: 24670634]

46. Goubran HA, Burnouf T, Radosevic M, El-Ekiaby M. The platelet-cancer loop. Eur J Intern Med. 2013;
47. Nagrath D, Caneba C, Karedath T, Bellance N. Metabolomics for mitochondrial and cancer studies. Biochim Biophys Acta. 2011;1807(6):650–63. [PubMed: 21420931]
48. Abrantes P, Rosa A, Francisco V, et al. Mitochondrial genome association study with peripheral arterial disease and venous thromboembolism. Atherosclerosis. 2016;252:97–105. [PubMed: 27513348]
49. Boudina S, Sena S, O'Neill BT, et al. Reduced mitochondrial oxidative capacity and increased mitochondrial uncoupling impair myocardial energetics in obesity. Circulation. 2005;112(17):2686–95. [PubMed: 16246967]
50. Boudina S, Sena S, Theobald H, et al. Mitochondrial energetics in the heart in obesity-related diabetes: direct evidence for increased uncoupled respiration and activation of uncoupling proteins. Diabetes. 2007;56(10):2457–66. [PubMed: 17623815]
51. Wilson PWF, D'Agostino RB, Sullivan L, Parise H, Kannel WB. Overweight and obesity as determinants of cardiovascular risk: the Framingham experience. Arch Intern Med. 2002;162(16):1867–72. [PubMed: 12196085]
52. Bhatt DL. What makes platelets angry: diabetes, fibrinogen, obesity, and impaired response to antiplatelet therapy? J Am Coll Cardiol. 2008;52(13):1060–1. [PubMed: 18848138]
53. Kutlucan A, Bulur S, Kr S, et al. The relationship between mean platelet volume with metabolic syndrome in obese individuals. Blood Coagul Fibrinolysis. 2012;23(5):388–90. [PubMed: 22473052]
54. Samocha-Bonet D, Justo D, Rogowski O, et al. Platelet counts and platelet activation markers in obese subjects. Mediators Inflamm. 2008;2008:834153. [PubMed: 18385810]
55. Sun N, Youle RJ, Finkel T. The Mitochondrial Basis of Aging. Mol Cell. 2016;61(5):654–666. [PubMed: 26942670]
56. Wiley CD, Velarde MC, Lecot P, et al. Mitochondrial Dysfunction Induces Senescence with a Distinct Secretory Phenotype. Cell Metab. 2016;23(2):303–14. [PubMed: 26686024]
57. Rowley JW, Oler AJ, Tolley ND, et al. Genome-wide RNA-seq analysis of human and mouse platelet transcriptomes. Blood. 2011;118(14):e101–e111. [PubMed: 21596849]
58. Schrepfer E, Scorrano L. Mitofusins, from Mitochondria to Metabolism. Mol Cell. 2016;61(5):683–694. [PubMed: 26942673]
59. Chen H, Chomyn A, Chan DC. Disruption of fusion results in mitochondrial heterogeneity and dysfunction. J Biol Chem. 2005;280(28):26185–26192. [PubMed: 15899901]
60. Chen S, Francioli LC, Goodrich JK, et al. A genome-wide mutational constraint map quantified from variation in 76,156 human genomes. bioRxiv. 2022;2022.03.20.485034.
61. Pleines I, Lebois M, Gangatirkar P, et al. Intrinsic apoptosis circumvents the functional decline of circulating platelets but does not cause the storage lesion. Blood. 2018;132(2):197–209. [PubMed: 29784641]
62. Mourier A, Motori E, Brandt T, et al. Mitofusin 2 is required to maintain mitochondrial coenzyme Q levels. J Cell Biol. 2015;208(4):429–42. [PubMed: 25688136]
63. Sowton AP, Millington-Burgess SL, Murray AJ, Harper MT. Rapid kinetics of changes in oxygen consumption rate in thrombin-stimulated platelets measured by high-resolution respirometry. Biochem Biophys Res Commun. 2018;503(4):2721. [PubMed: 30093113]
64. Kulkarni PP, Tiwari A, Singh N, et al. Aerobic glycolysis fuels platelet activation: small-molecule modulators of platelet metabolism as anti-thrombotic agents. Haematologica. 2019;104(4):806. [PubMed: 30381300]
65. Remenyi G, Szasz R, Friese P, Dale GL. Role of mitochondrial permeability transition pore in coated-platelet formation. Arterioscler Thromb Vasc Biol. 2005;25(2):467–471. [PubMed: 15591217]
66. Choo HJ, Saafir TB, Mkumba L, Wagner MB, Jobe SM. Mitochondrial calcium and reactive oxygen species regulate agonist-initiated platelet phosphatidylserine exposure. Arterioscler Thromb Vasc Biol. 2012;32(12):2946. [PubMed: 23087357]
67. Nagy Z, Vögtle T, Geer MJ, et al. The Gp1ba-Cre transgenic mouse: a new model to delineate platelet and leukocyte functions. Blood. 2019;133(4):331–343. [PubMed: 30429161]

68. Wei Y, Tejera P, Wang Z, et al. A missense genetic variant in LRRC16A/CARMIL1 improves acute respiratory distress syndrome survival by attenuating platelet count decline. Am J Respir Crit Care Med. 2017;195(10):1353–1361. [PubMed: 27768389]

69. Sjövall F, Morota S, Hansson MJ, et al. Temporal increase of platelet mitochondrial respiration is negatively associated with clinical outcome in patients with sepsis. Crit Care. 2010;14(6):.

70. Gründler K, Angstwurm M, Hilge R, et al. Platelet mitochondrial membrane depolarization reflects disease severity in patients with sepsis and correlates with clinical outcome. Crit Care. 2014;18(1):R31. [PubMed: 24521521]

71. Montenont E, Bhatlekar S, Jacob S, et al. CRISPR-edited megakaryocytes for rapid screening of platelet gene functions. Blood Adv. 2021;5(9):2362. [PubMed: 33944898]

72. Simon LM, Chen ES, Edelstein LC, et al. Integrative Multi-omic Analysis of Human Platelet eQTLs Reveals Alternative Start Site in Mitofusin 2. Am J Hum Genet. 2016;98(5):883–97. [PubMed: 27132591]

73. Fidler TPTP, Middleton EA, Rowley JWJW, et al. Glucose Transporter 3 Potentiates Degranulation and Is Required for Platelet Activation. Arterioscler Thromb Vasc Biol. 2017;37(9):1628–1639. [PubMed: 28663252]

74. Chen H, McCaffery JM, Chan DC. Mitochondrial fusion protects against neurodegeneration in the cerebellum. Cell. 2007;130(3):548–62. [PubMed: 17693261]

75. Tiedt R, Schomber T, Hao-Shen H, Skoda RC. Pf4-Cre transgenic mice allow the generation of lineage-restricted gene knockouts for studying megakaryocyte and platelet function in vivo. Blood. 2007;109(4):1503–6. [PubMed: 17032923]

76. Dwivedi AK, Mallawaarachchi I, Alvarado LA. Analysis of small sample size studies using nonparametric bootstrap test with pooled resampling method. Stat Med. 2017;36(14):2187–2205. [PubMed: 28276584]

77. Dewey M metap: meta-analysis of significance values. 2022;

Novelty and Significance

What Is Known?

- Elevated platelet counts or platelet reactivity increase risk for platelet clots, while lower platelet counts or reactivity increase bleeding tendencies.
- Genome wide association studies (GWAS) have associated variants in Mitofusin-2 (*MFN2*) with platelet count.
- MFN2 regulates mitochondrial shape and function across different cell types.

What New Information Does This Article Contribute?

- MFN2 regulates mitochondrial funciton in megakaryocytes and platelets and contributes to platelet lifespan.
- Loss of platelet Mfn2 reduces various platelet activation responses, decreases infarct size after ischemic stroke in mice, and aggravates inflammatory bleeding in an LPS-induced acute lung injury model.
- *MFN2* variants are associated with ARDS mortality.

Changes in platelet counts and activity contribute to various human diseases, especially those related to bleeding and clotting. Genetic studies have associated the mitochondrial fusion protein MFN2 with platelet counts, but underlying mechanisms linking MFN2 with platelet biology have not been identified. Mitochondrial size and shape in cells is dynamic, and MFN2 mediates the fusion of mitochondria into interconnected organelles to maintain and promote mitochondrial functions. Our data using human cells and murine models show that MFN2 mediates mitochondrial fusion in megakaryocytes, the precursor cell of platelets. Loss of MFN2 in megakaryocytes impairs mitochondrial functions in platelets, and accelerates platelet death, especially in older platelets. Loss of MFN2 also results in altered platelet activity, reduced stroke size following ischemia-reperfusion injury in mice, and increased bleeding in a mouse model of lung injury. In summary, these findings uncover a role for MFN2-mediated mitochondrial dynamics in shaping platelet numbers and function, and implicate MFN2 involvement in diseases such as stroke and acute lung injury.

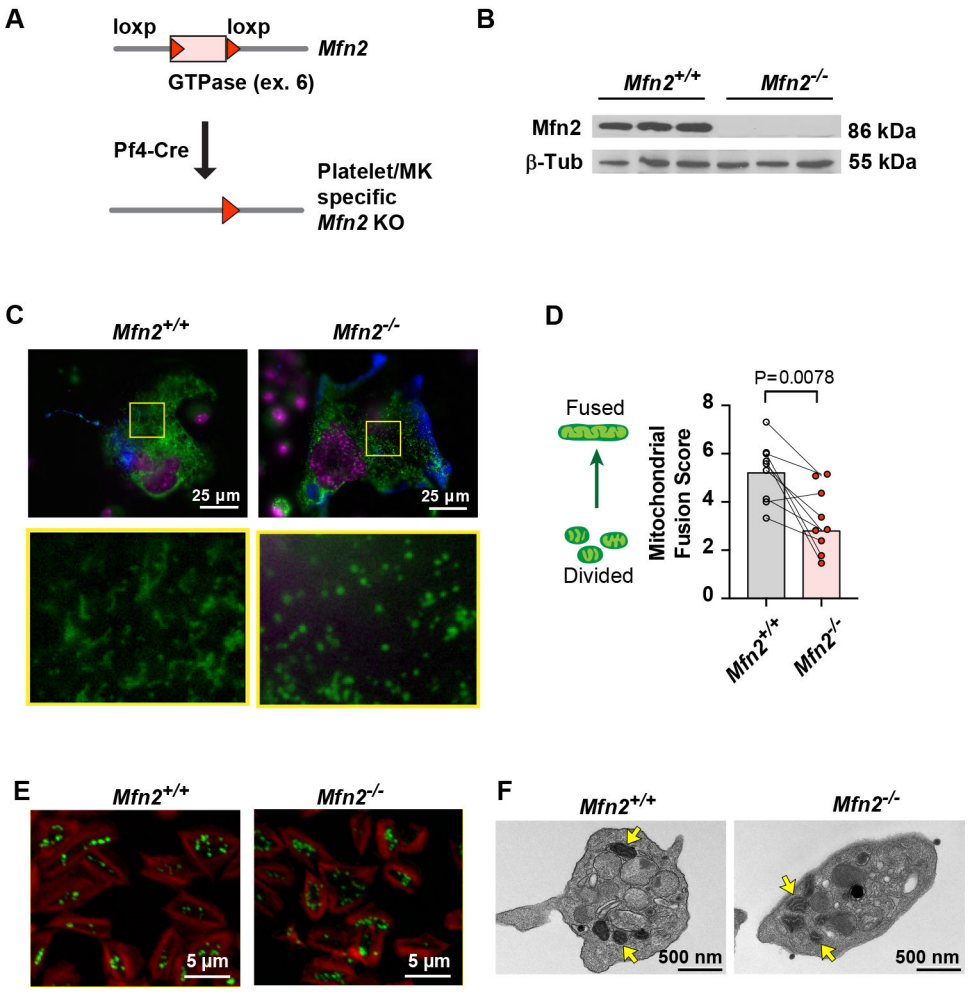

Figure 1: Mitochondrial morphology in platelets and MK from Pf4-CRE conditional *Mfn2* knockout mice

A. Transgenic Pf4 promoter-driven Cre recombinase[75] mice were crossed with mice harboring homozygous floxed Mfn2[74] to generate platelet/MK specific Mfn2 knockout mice (called $Mfn2^{-/-}$). **B**. Representative western blot for Mfn2 in platelets from $Mfn2^{+/+}$ and $Mfn2^{-/-}$ mice. **C.** Representative live immunofluorescent microscopy images of mitochondrial morphology in MKs derived from the bone marrow of $Mfn2^{+/+}$ and $Mfn2^{-/-}$ mice isolated and cultured in pairs. MKs are marked with surface GPIbα staining (blue); mitochondria (mitotracker, green) and nuclei (Hoechts, magenta) are stained with live cell penetrating dyes. Bottom panels are magnified portions of the top panels outlined by the yellow boxes. **D**. Overall mitochondria morphology in individual MKs was scored for fusion on a scale of 1-10 by an observer blinded to genotype as described in detail in the methods. Briefly, higher scores are given for MKs with predominantly elongated and branched mitochondria and low scores for predominantly punctate, single mitochondria. On average 15 MKs were scored per sample and >250 MKs were scored in total (Wilcoxon paired sign rank test, N=9 culture pairs per group). **E**. Representative confocal immunofluorescent microscopy images of mitochondrial morphology in platelets from $Mfn2^{+/+}$ and $Mfn2^{-/-}$ mice stained with mitotracker (green) and phalloidin (cytoskeleton, red). **F**. Representative

TEM sections of platelets from *Mfn2*$^{+/+}$ and *Mfn2*$^{-/-}$ mice. Arrows point to mitochondria. Most mitochondria were round or oval in shape, but occasional mitochondria were elongated (see Supplement Figure 3 for additional images and quantitation).

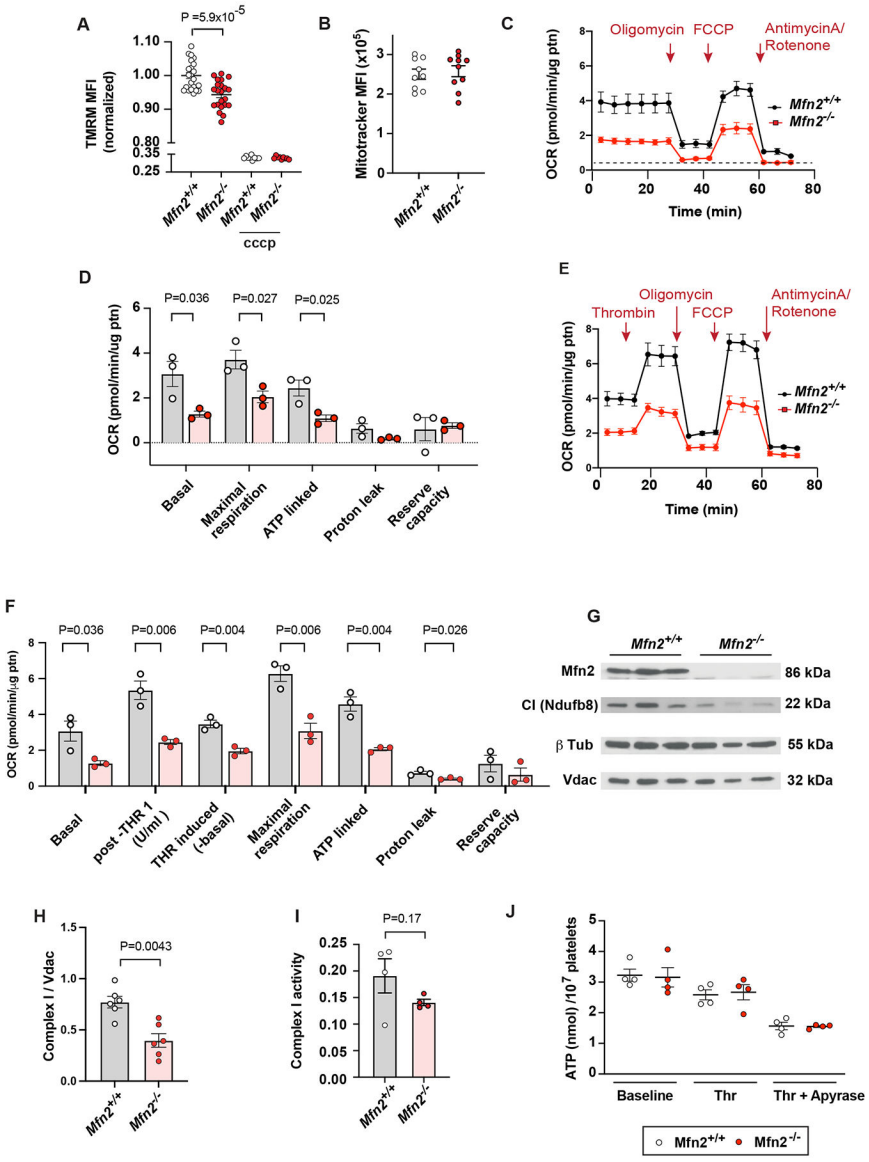

Figure 2: Mfn2$^{-/-}$ impairs mitochondrial function.

A. Mitochondrial membrane potential in platelets (gated on FSC/SSC and CD41+) from *Mfn2*$^{+/+}$ and *Mfn2*$^{-/-}$ mice as measured by flow cytometry analysis of TMRM staining. Measurements were taken before and after treatment with CCCP which depolarizes mitochondria. See Supplement Figure 4A for representative flow cytometry histograms. t-test, N=22 per group (10 males, 12 females). **B.** Mitochondrial load measured by Mitotracker in *Mfn2*$^{+/+}$ and *Mfn2*$^{-/-}$ platelets (N=9 *Mfn2*$^{+/+}$ and N=10 *Mfn2*$^{-/-}$) **C**. Representative experiment (of 5 independent experiments with a total of n=14 independent mice per group, see Supplement 4C for pooled, normalized data from all experiments) for Oxygen Consumption Rate (OCR) in untreated *Mfn2*$^{+/+}$ and *Mfn2*$^{-/-}$ platelets as measured by Seahorse at baseline, and following treatment with Oligomycin (ATP synthase inhibitor to identify cellular ATP production); FCCP (uncoupling agent that disrupts membrane potential to determine maximal respiration); Rotenone and Antimycin A (Complex I and

III inhibitors to define mitochondrial specific OCR). **D**. summary of seahorse measurements in C. See Supplement Figure 2B for how these measurements are derived. t tests, N=3 per group. **E**. OCR in *Mfn2*$^{+/+}$ and *Mfn2*$^{-/-}$ platelets treated with 1 U/mL thrombin and treatments with mitochondrial modulators (described for B) at the time points indicated in C. **F.** Summary of Seahorse measurements in E. t tests, N=3 per group. **G**. Representative western blot of an index mitochondrial complex I nuclear encoded subunit Ndufb8 (labile when complex I is not assembled) compared to beta tubulin (cytoskeletal) and Vdac (nuclear encoded mitochondrial channel protein). **H**. Densitometry analysis of complex I/Vdac protein levels in platelets *Mfn2*$^{+/+}$ and *Mfn2*$^{-/-}$ mice. Mann-Whitney test, N=5 per group. **I**. Mitochondrial complex I activity measured in lysates from male *Mfn2*$^{+/+}$ and *Mfn2*$^{-/-}$ platelets. Mann-Whitney test, N=4 per group. **J**. Stored ATP content in *Mfn2*$^{+/+}$ and *Mfn2*$^{-/-}$ platelets before and after stimulation with thrombin or thrombin plus apyrase (to separate intracellular from stored/released ATP).

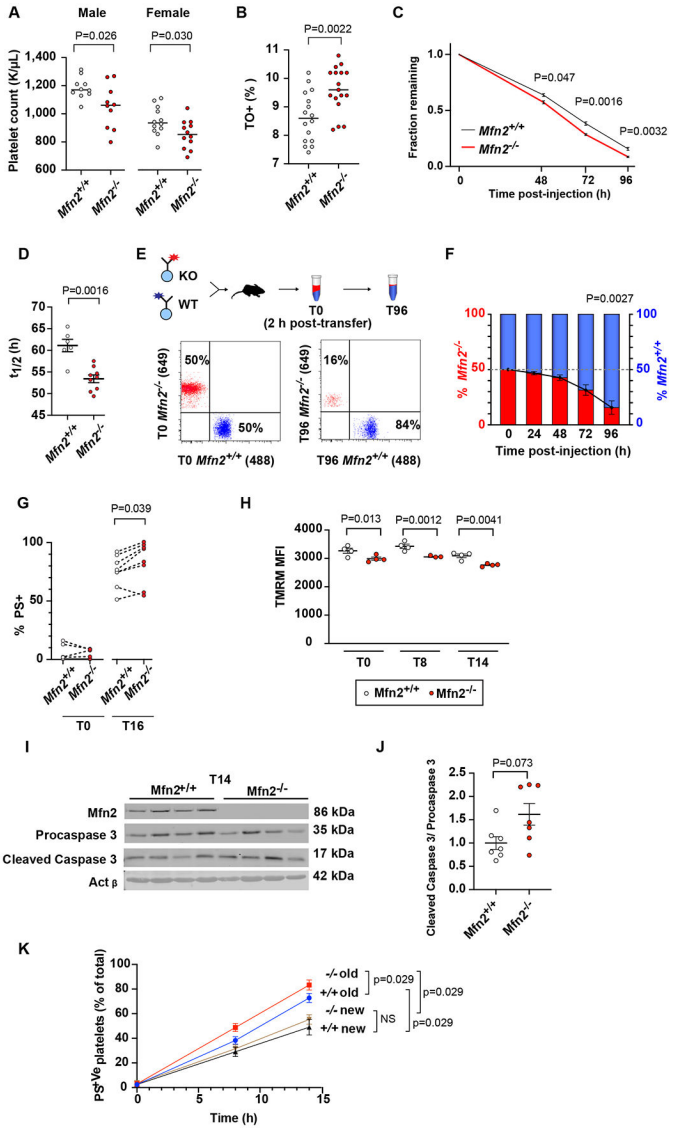

Figure 3: Conditional platelet/MK deletion of Mfn2 reduces platelet counts and platelet lifespan through accelerated apoptosis of older platelets.

A. Platelet counts in 2-month-old male and female *Mfn2*$^{+/+}$ and *Mfn2*$^{-/-}$ littermate mice (t-test, N=10-12 per group). **B**. Thiazole orange staining of reticulated platelets as measured by flow cytometry in 5-month-old *Mfn2*$^{+/+}$ and *Mfn2*$^{-/-}$ littermate mice (t test, N=16-17 per group). **C.** Mice were injected with Dylight 488-GPIbα and the fraction of Dylight labeled platelets of CD41+ platelets was assessed by flow cytometry in whole blood obtained by repeated tail pricks in the same mouse at the indicated time points starting 4 h after injection (set as T0). **D.** Calculated platelet half-life from **C** (C-D: Mann-Whitney tests, N=6-7 per group). **E**. Schematic summary and representative flow plots of platelet transfusion mixing experiment. Platelets in *Mfn2*$^{-/-}$ and *Mfn2*$^{+/+}$ mice were differentially prelabeled by intravenous injection of Dylight 488 or Dylight 649 anti-platelet fab fragment. Two hours later blood was drawn, and *Mfn2*$^{-/-}$ and *Mfn2*$^{+/+}$ PRP were mixed 1:1 and injected intravenously into recipient mice. Blood was drawn at 2 h for baseline (T0), then 24, 48, and

96 h later and the percent of *Mfn2*$^{-/-}$ vs *Mfn2*$^{+/+}$ platelets determined by flow cytometry. Shown are representative flow plots showing the percent of *Mfn2*$^{-/-}$ and *Mfn2*$^{+/+}$ platelets at T0 and T96. **F**. Summary of the fraction of *Mfn2*$^{-/-}$ (red) and *Mfn2*$^{+/+}$ (blue) remaining at different time points post injection. Shown is a representative of 3 independent experiments. *Mfn2*$^{-/-}$ platelets disappeared faster than *Mfn2*$^{+/+}$ platelets after transfusion regardless of whether the labels were swapped (not shown) or recipients were *Mfn2*$^{+/+}$ or *Mfn2*$^{-/-}$ mice: Experiment 1: 4 *Mfn2*$^{+/+}$ and 4 *Mfn2*$^{-/-}$ (2 each male/female) mixed and transfused into 4 *Mfn2*$^{+/+}$ and 4 *Mfn2*$^{-/-}$, p=0.08; Experiment 2: 7 *Mfn2*$^{+/+}$ males and 7 *Mfn2*$^{-/-}$ males mixed and transfused into 3 *Mfn2*$^{+/+}$ and 4 *Mfn2*$^{-/-}$ mice, p=0.02; Experiment 3: 7 *Mfn2*$^{+/+}$ and 7 *Mfn2*$^{-/-}$ females mixed and transfused into 7 recipients, p=0.003. **G**. *Mfn2*$^{+/+}$ and *Mfn2*$^{-/-}$ platelets differentially labeled and mixed as in C were stained with annexin V and analyzed by flow cytometry immediately (T0) or following *ex vivo* co-culture for 16 h at 37° C. The dotted lines indicate the respective *Mfn2*$^{+/+}$ and *Mfn2*$^{-/-}$ pairs that were mixed in the same tube (Wilcoxon paired sign rank test, N=7). **H.** Mitochondrial potential (TMRM) in *ex vivo* cultured platelets. **I-J.** Western blot and densitometry analysis for cleaved caspase 3 and procaspase 3 in Mfn2$^{+/+}$ and Mfn2$^{-/-}$ platelets after 14h *ex vivo* at 37° C (Mann-Whitney test, N=7 per group) **K**. Dylight was injected into mice 72 h prior to isolation to distinguish old from new platelets. Annexin V staining assessed by flow cytometry at 0 (T0), 8 h (T8), and 14 h (T14) on new (Dylight negative) and old (Dylight positive) platelets (Mann-Whitney tests for AUC, N=4-6 per group).

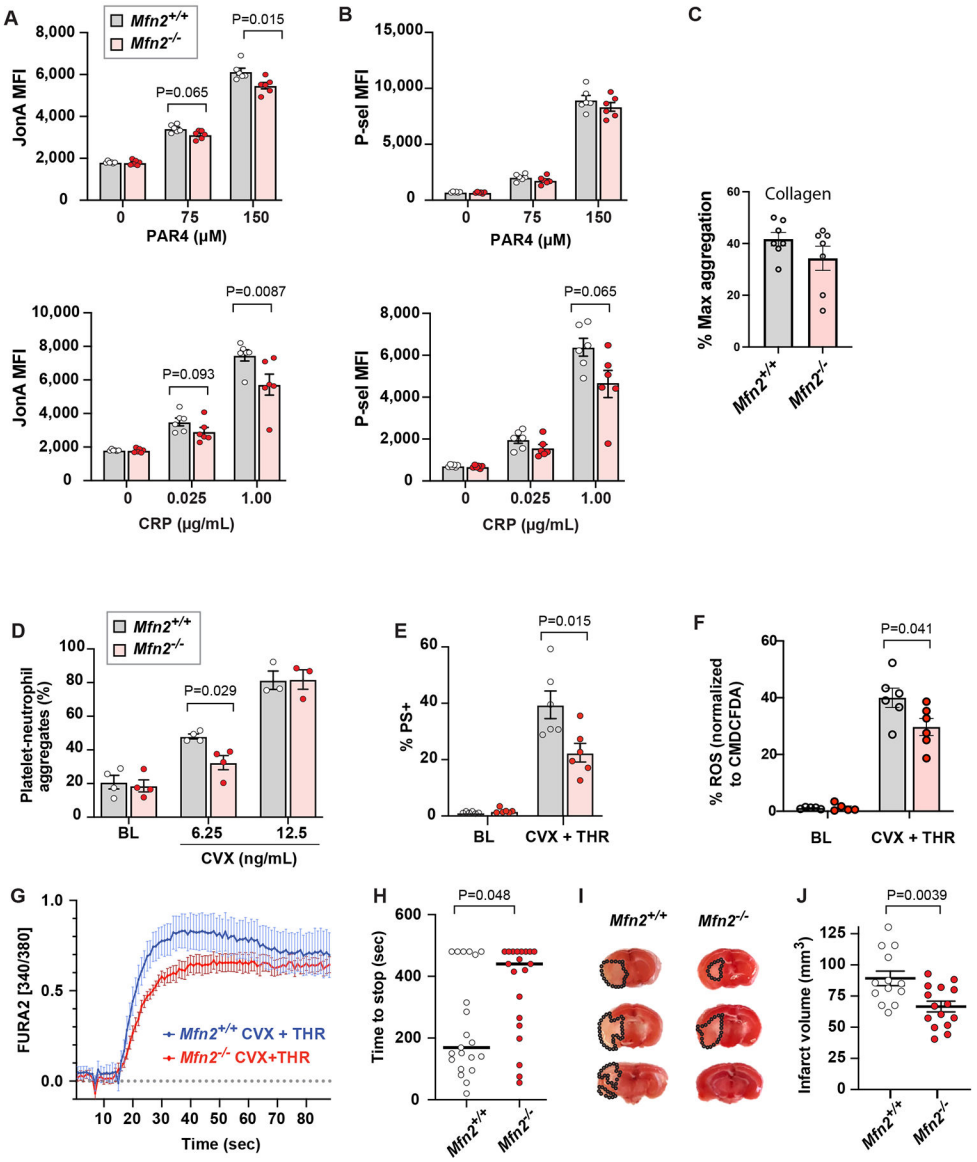

Figure 4: *Mfn2*$^{-/-}$ alters platelet activation, hemostasis, and thrombosis.

A-B. Flow cytometry analysis of platelet activation assessed by surface binding of **A.** Jon/A (activated αIIb/β3) or **B.** anti-p-selectin antibody (degranulation) at baseline or after 10 min incubation with indicated doses of PAR4 (thrombin receptor) or CRP (GPVI receptor) agonists (t test, N=6 per group). **C.** Aggregation of washed platelets, normalize to counts, in response to collagen (Mann-Whitney test, N=7 per group). **D**. Platelet-neutrophil aggregates in *Mfn2*$^{+/+}$ and *Mfn2*$^{-/-}$ whole blood at baseline and in response to convulxin (Mann-Whitney test, N=3-4 per group). **E**. Flow cytometry analysis of PS exposure (annexin V binding) on the surface of platelets at baseline and after activation with dual agonist thrombin (0.1 U/mL) + convulxin (500 ng/mL) (Mann-Whitney test, N=6 per group). **F**. ROS generation in *Mfn2*$^{+/+}$ and *Mfn2*$^{-/-}$ platelets in response to thrombin (0.1 U/mL) + convulxin (500 ng/mL) (Mann-Whitney test, N=6 per group). **G**. Ca^{2+}cyt transients in *Mfn2*$^{+/+}$ and *Mfn2*$^{-/-}$ platelets after stimulation with thrombin (0.1 U/mL) + convulxin (500

ng/mL). N=9 per group. **H**. Time to cessation of bleeding after tail resection in *Mfn2*$^{+/+}$ and *Mfn2*$^{-/-}$ mice. Each point represents an individual mouse. (Mann Whitney test, N=20-21 per group). **I**. Representative images of brains from mice after ischemia/reperfusion injury in *Mfn2*$^{+/+}$ (left) and *Mfn2*$^{-/-}$ (right) mice. Infarcts are outlined with dotted lines. **J**. Summary of infarct volume. t-test, N=13-15 mice per group.

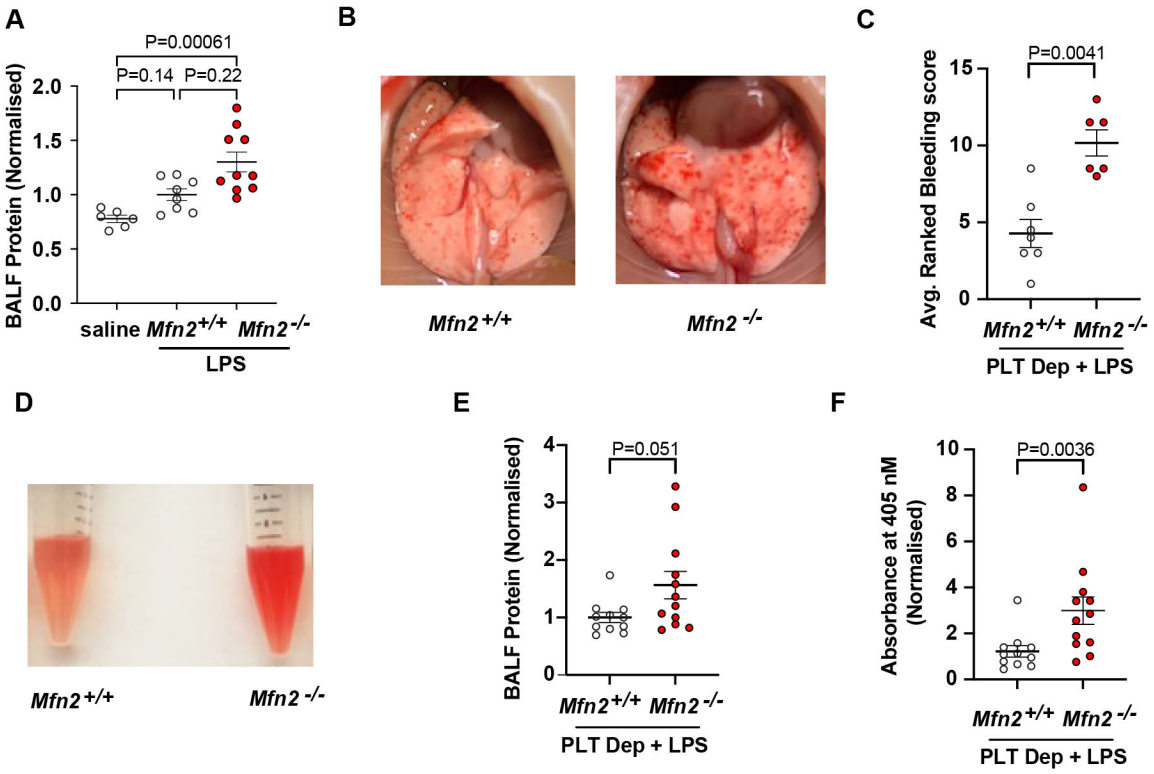

Figure 5: Mfn2$^{-/-}$ increases lung vascular permeability and aggravates inflammatory bleeding in LPS-induced acute lung injury model.

A. Protein concentration in the BALF of *Mfn2*$^{+/+}$ and *Mfn2*$^{-/-}$ mice 24 h post-intratracheal saline or LPS-challenge (1.6 mg/Kg body weight). Kruskal Wallis test with Dunn's multiple (3) comparisons, n=8-10 mice per group. **B.** Representative images of lungs from thrombocytopenic *Mfn2*$^{+/+}$ and *Mfn2*$^{-/-}$ mice 24 h post-intratracheal LPS-challenge (1.6 mg/Kg body weight). **C.** Bleeding score of lungs from thrombocytopenic *Mfn2*$^{+/+}$ and *Mfn2*$^{-/-}$ mice 24 h post-intratracheal LPS-challenge. The lungs were scored for bleeding by two observers blinded to genotype and averaged. Higher scores were given to lungs with increased bleeding. Mann Whitney test, n=5-7 mice per group. **D.** Representative images (N=11) of BALF from thrombocytopenic *Mfn2*$^{+/+}$ and *Mfn2*$^{-/-}$ mice 24 h post-intratracheal LPS-challenge (1.6 mg/Kg body weight). **E.** Protein concentration in the BALF of *Mfn2*$^{+/+}$ and *Mfn2*$^{-/-}$ thrombocytopenic mice 24 h post-intratracheal LPS-challenge (1.6 mg/Kg body weight). Mann-Whitney test, n=11-12 per group. **F.** BALF hemoglobin as a measure of RBC infiltration in the lungs of thrombocytopenic *Mfn2*$^{+/+}$ and *Mfn2*$^{-/-}$. Mann-Whitney test, n=11-12 per group.

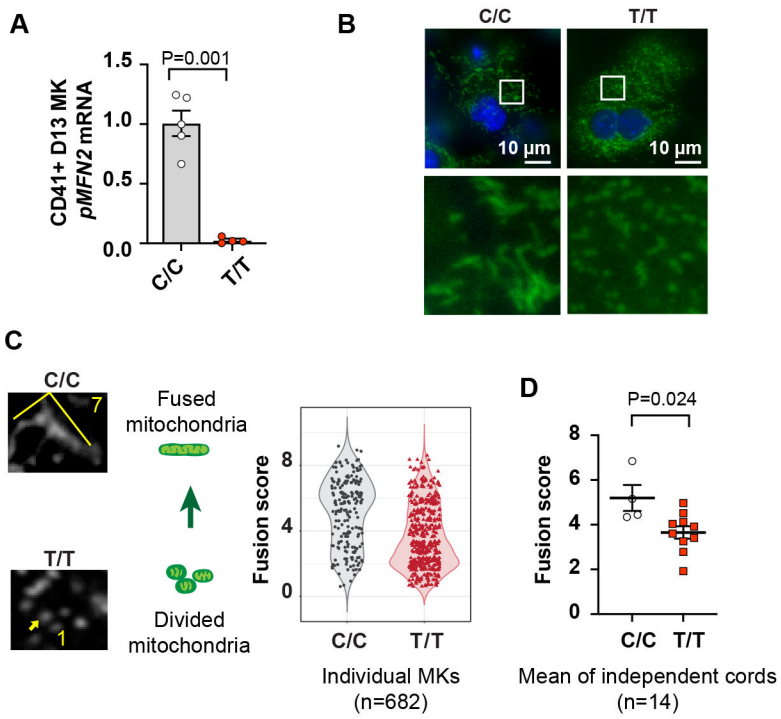

Figure 6: *pMFN2* eQTL affects *MFN2* expression and mitochondrial morphology in human cord blood (CB) megakaryocytes (MKs).

A. *pMFN2* mRNA normalized to *GAPDH* mRNA in day13 CB MKs from rs1474868 C/C, C/T and T/T individuals as measured by real time PCR (nonparametric bootstrap test, 1000 resamples), N=5 C/C or C/T and N=4 T/T). **B**. Representative live immunofluorescent microscopy images of mitochondria (mitotracker, green) and nuclei (Hoechts, blue) in day 13 CB MKs of the indicated rs1474868 genotype, showing more elongated mitochondria in C/C MKs and more punctate mitochondria in T/T MKs. Bottom panels are magnified portions of the top panels outlined by the white boxes. **C**. Mitochondrial fusion scores for CB MKs with the indicated rs1474868 genotype were scored for fusion on a scale of 1-10 by an observer blinded to genotype as described in detail in the methods. Representative images of mitochondria from MKs with different scores are shown on the left. Individual MK scores are shown in the violin and average scores per cord are shown in **D** (Mann-Whitney test, N=4 C/C and N=10 T/T).

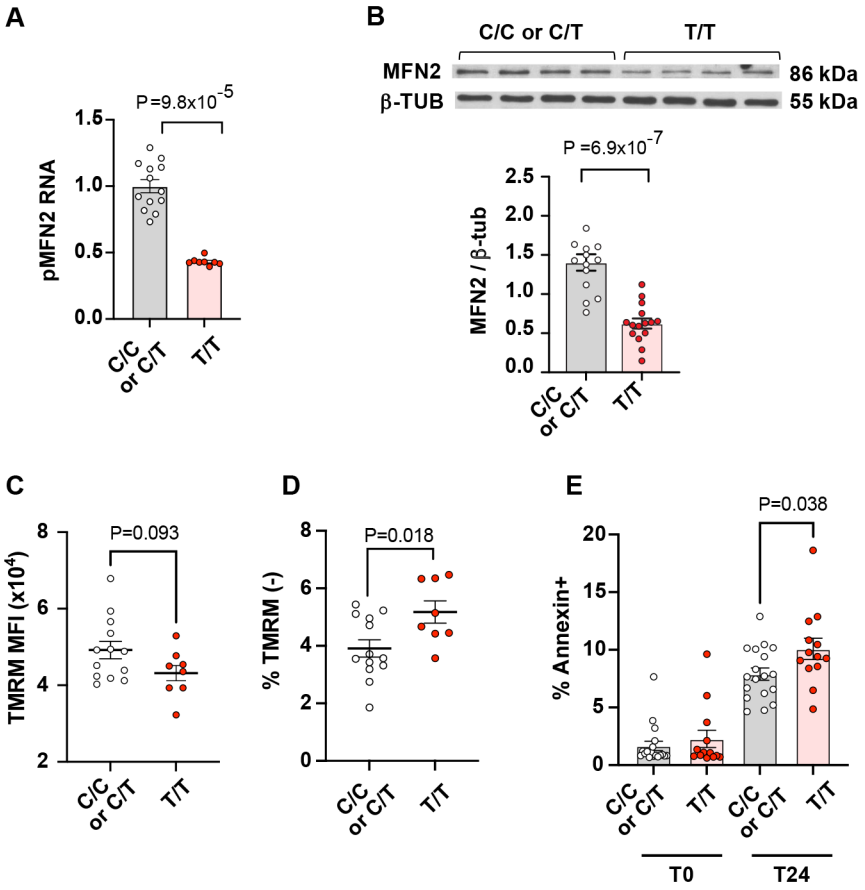

Figure 7: *pMFN2* eQTL affects MFN2 protein and *ex vivo* survival of human platelets.

A. Real time PCR analysis of *pMFN2* expression in platelets from individuals with rs1474868 C/C, C/T or T/T genotypes normalized to *GAPDH* mRNA (Mann Whitney test, C/C or C/T N=13; T/T N=8). **B.** Top: representative western blot of MFN2 protein in platelets from individuals with the indicated rs1474868 genotypes. Beta Tubulin is used as loading control. Bottom: densitometric analysis of all samples (t test, C/C or C/T N=13; T/T N=15). **C.** Mitochondrial potential ($\Delta\Psi_M$) measured as TMRM MFI in washed platelets (gated on FSC/SSC and CD41) from rs1474868 C/C or C/T versus T/T individuals (t test, C/C or C/T N=13; T/T N=8). **D.** Loss of mitochondrial potential ($\Delta\Psi_M$) measured as % TMRM negative (-) platelets from rs1474868 C/C or C/T versus T/T individuals (t test, C/C or C/T N=13; T/T N=8). **E.** Resting PS exposure measured as % annexin V on washed platelets from rs1474868 C/C or C/T versus T/T individuals at time 0 (T0) and after 24 h (T24) incubation at 37° (t test, N=18 C/C or C/T and N=13 T/T). Results in panels C-E are from a cohort of donors recruited in 2018. See Supplement Figure 9 for TMRM, PS exposure, and Caspase-3 activity over 48 hours in an independent cohort recruited in 2023. Meta-analysis of combined p-values for both cohorts (P_s, Stouffer's method, 2 tailed): median TMRM P_s=0.040 (P_1=0.093, P_2=0.125); % TMRM- P_s=0.023 (P_1=0.018, P_2=0.31); Annexin at T24 P_s=0.048 (P1=0.038, P2=0.35).